

Coexistence and Spectrum Sharing Above 100 GHz

Michele Polese, *Member, IEEE*, Xavier Cantos-Roman, *Graduate Student Member, IEEE*,
Arjun Singh, *Member, IEEE*, Michael J. Marcus, *Fellow, IEEE*, Thomas J. Maccarone,
Tommaso Melodia, *Fellow, IEEE*, and Josep M. Jornet, *Senior Member, IEEE*

Abstract—The electromagnetic spectrum plays a fundamental role for the development of the digital society. It enables wireless communications (either between humans or machines) and sensing (for example for Earth exploration, radio astronomy, imaging, and radars, among others). While each of these uses benefits from a larger bandwidth, the spectrum is a finite resource. This introduces competing interests among the different stakeholders of the spectrum, which have led—so far—to rigid policies and spectrum allocations. Recently, the spectrum crunch in the sub-6 GHz bands has prompted communication technologies to move to higher carrier frequencies, where future 6G wireless networks can exploit theoretically very large bandwidths. However, the spectrum above 100 GHz features several narrow, yet numerous sub-bands that are exclusively allocated for passive sensing applications, e.g., for climate and weather monitoring. This prevents the allocation of large contiguous bands to active users of the spectrum, either being communications (which need tens of gigahertz of bandwidth to target terabit-per-second links) or radars. This paper explores how spectrum policy and spectrum technologies can evolve to enable *sharing* among different stakeholders in the above 100 GHz spectrum, without introducing harmful interference or disrupting either security applications or fundamental science exploration. This portion of the spectrum presents new challenges and opportunities for the design of spectrum sharing schemes, including higher spreading and absorption losses, extremely directional antenna technologies, and ultra-high data-rate communications, among others. The paper provides a tutorial on current regulations above 100 GHz, and highlights how sharing is central to allowing each stakeholder to make the most out of this spectrum. It then defines—through detailed simulations based on standard International Telecommunications Union (ITU) channel and antenna models—scenarios in which active users may introduce harmful interference to passive sensing. Based on this evaluation, it reviews a number of promising techniques that can enable active/passive sharing above 100 GHz. The critical review and tutorial on policy and technologies of this paper have the potential to kickstart future research and regulations that promote safe coexistence between active and passive users above 100 GHz, further benefiting the development of digital technologies and scientific exploration.

Index Terms—Terahertz Communication; Sub-millimeter-waves; Spectrum Sharing; Passive users; Coexistence; 6G

I. INTRODUCTION

The digital society of the next decade will increasingly rely on services provided by a fundamental, invisible, yet scarce

M. Polese, X. Cantos-Roman, M. J. Marcus, T. Melodia, and J. M. Jornet are with the Institute for the Wireless Internet of Things and with the Department of Electrical and Computer Engineering, Northeastern University, Boston, MA, USA.

A. Singh is with the Department of Engineering at the State University of New York Polytechnic Institute, Utica, NY, USA.

T. J. Maccarone is with the Department of Physics & Astronomy, Texas Tech University, Lubbock, TX, USA.

This work was partially supported by NSF under Grants AST-2037896, MPS-2037890, CNS-2011411, and CNS-2225590.

resource, i.e., the electromagnetic spectrum. The wireless spectrum enables a diverse set of applications, from high-speed communications [1], to imaging [2], remote sensing [3], Earth and space exploration [4], and radio astronomy [5]. Radio Frequency (RF) technologies, either communications or sensing, generally benefit from using a larger bandwidth, with a proportional improvement to the capacity and/or the sensing resolution [6], [7]. The finite nature of the spectrum, however, translates into limited availability of resources for each use case, prompting researchers to expand into new, unexplored portions of the spectrum, and to investigate sharing mechanisms. Notably, the crowded spectrum in the traditional sub-6 gigahertz (GHz) band has led 5th Generation (5G) networks as well as radars and sensing systems to use the lower millimeter wave (mmWave) band. For example, 3rd Generation Partnership Project (3GPP) NR, a 5G technology, is expected to use carrier frequencies as high as 71 GHz [8], while radars generally operate in multi-GHz bands around 60 GHz and 77 GHz [9]. Similarly, policies and technologies have evolved to accommodate shared uses of the spectrum [10].

As the design and engineering of antennas and RF circuitry for high-frequency transceivers and sensors has improved, the spectrum above 100 GHz has entered the spotlight as an enabler of 6th Generation (6G) communications technologies, on the one side [11], and of more advanced sensing solutions, on the other [12]. This portion of the spectrum includes large chunks of unused bandwidth, which both sensing and communications can benefit from.

Notably, certain sensing techniques integrate a large number of observations over time and frequency. As per the central limit theorem, the accuracy of the measurement is proportional to the square root of the number of observations [5]. Given a certain noise level target, a larger bandwidth allows measurements to be collected in a shorter time period, which is particularly beneficial in case of dynamic sources or measurement setups. Similarly, radars can provide more precise tracking with a larger bandwidth [13]. Additionally, the spectrum above 100 GHz features specific sub-bands of interest to the scientific community, because of molecular transitions [4], [14]. Finally, larger bandwidth enables higher data rates for communications, with tens of GHz needed to target the terabit-per-second (Tbps) data rate goal of future 6G networks [15], [16], as we discuss later in this paper. The need for ultra-high data rates is also shared by the scientific community, to overcome limitations introduced by low capacity telemetry links between sensing satellites in space and ground stations [17].

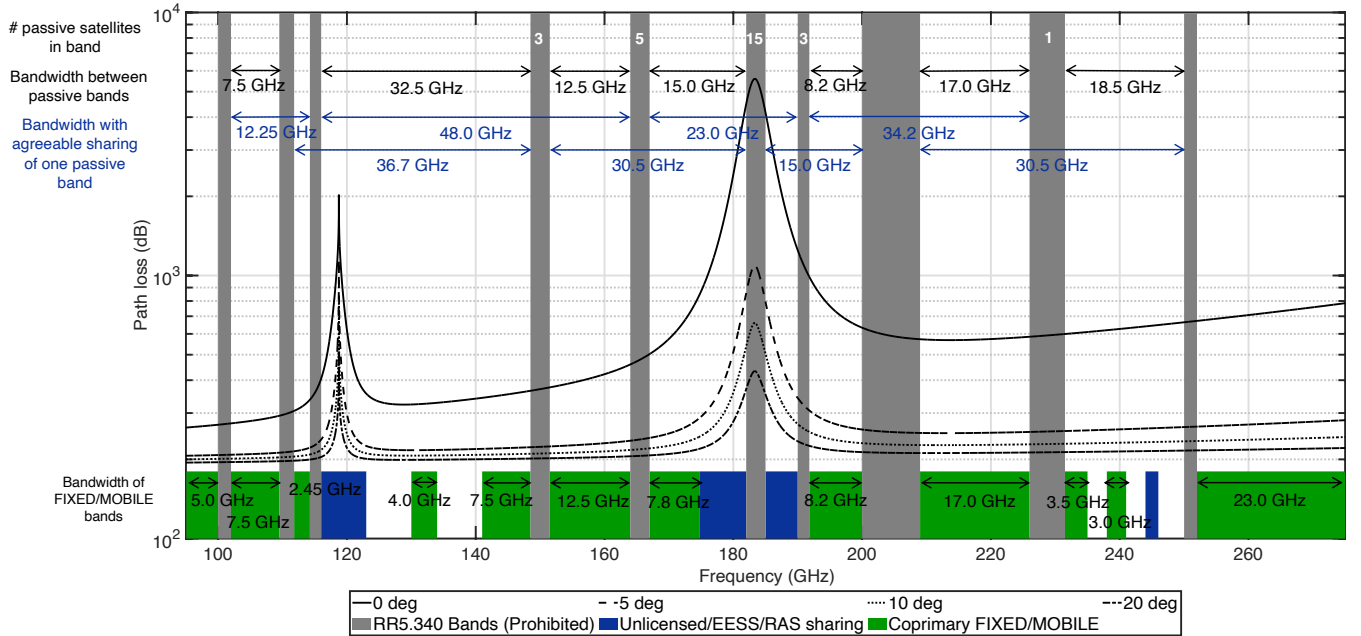


Figure 1: Spectrum allocation above 100 GHz and the path loss for a 407 km Earth-space link with different elevation angles, based on the channel model discussed in Section IV. The figure also describes existing services and spectrum allocation based on the International Telecommunications Union (ITU) radio regulations [18], and includes the number of passive satellites in each band dedicated to passive sensing. Finally, the top part of the figure reports the chunks of bandwidth that are available between passive bands (black) or by enabling sharing of one passive band (blue).

A. Sharing the Spectrum in the 21st Century

As a consequence, *both sensing and communications communities have a stake in the spectrum above 100 GHz*, either because of the availability of large chunks of untapped bandwidth, or because of specific frequencies of interest. The different communities, however, often express different needs with respect to how the spectrum should be used. For example, even modest levels of Radio Frequency Interference (RFI) can strongly affect the performance of most classes of passive sensing systems [19], while communications or other sensing techniques (e.g., some radars) need active transmissions. This has led national and international spectrum regulation entities to define a rigid allocation scheme in the spectrum above 100 GHz, with a set of narrow, yet numerous sub-bands exclusively dedicated to passive sensing (i.e., for science and space exploration) [18]. While the total bandwidth reserved for passive users is rather small (i.e., 33.35 GHz between 100 and 275 GHz), the positioning of these sub-bands in the overall spectrum prevents the allocation of large chunks of contiguous bandwidth for active usage. As highlighted in Figure 1, the largest contiguous chunk allocated to active users between 100 and 275 GHz has a bandwidth of 32.5 GHz (between 116 GHz and 148.5 GHz). However, in this band, only 12.25 GHz (non contiguous) are allocated to fixed and mobile communications (i.e., 122.25-123 GHz, 130-134 GHz, 141-148.5 GHz), and the remaining 19.5 GHz are earmarked for active sensing techniques, radionavigation, and radiolocation. For communications, this is less than the bandwidth that is

typically needed to achieve the 1 Tbps target rate of future 6G networks. Similarly, the needs of the sensing community have evolved since when the current regulatory approach was established. At that time, the electronics for sensing systems were severely limited in terms of the bandwidth they could handle, and millimeter band astronomy facilities were not sensitive enough to see molecular features at large distances, where the expansion of the Universe changes their wavelengths substantially. All of these aspects of the situation have now changed, so that the current approach of protecting narrow bands everywhere all the time is no longer as valuable as protecting broader bands at specific places and times.

Therefore, a dynamic and shared use of the spectrum above 100 GHz will simultaneously enable next-generation sensing *and* communication technologies. Spectrum sharing has proven a successful enabler of advanced spectrum usage in the sub-6 GHz and lower mmWaves bands. A notable example is that of the Citizen Broadband Radio Service (CBRS) band, i.e., 150 MHz between 3.55 GHz to 3.7 GHz which have been repurposed for shared usage between sensing systems (e.g., U.S. Navy radars), critical communications (to and from aircrafts), and commercial users [20], [21]. According to the recent regulations for CBRS, secondary users (generally, commercial ones) need to preempt spectrum usage and effectively avoid RFI to the primary users. This shows that it is possible to go beyond a strict resource partitioning scheme with exclusive spectrum access, with a mutually beneficial outcome, i.e., more bandwidth can be *dynamically* allocated to different services

according to need. Along this line, a National Research Council report [22] shows that—with proper coordination—a constellation of 30 sensing satellites and active users on the ground can share the same bands with active transmissions for 99.7% of the time and without any interference to the passive sensing system. The ITU has also advanced a resolution at the World Radio Conference (WRC) in 2000 to promote sharing of the passive bands above 71 GHz, as long as sharing does not expose passive services to interference levels beyond those standardized by ITU [23]–[26].

The characteristics of devices and propagation in the above 100 GHz introduce new opportunities and challenges with respect to spectrum sharing approaches in the sub-6 GHz band [27], considering approaches that are based on device design, signal processing at the physical layer, and coordination at the Medium Access Control (MAC) and above. The higher spreading and absorption losses above 100 GHz [11], together with directional transceiver architectures [28], allow for increased spatial reuse and coexistence. Similarly, a larger bandwidth can shorten the observation time for sensing and the transmission time for communications, thus potentially enabling more refined and flexible time-sharing strategies. At the same time, however, the device and RF circuit design is made more challenging by the high carrier frequency and large bandwidth processing requirements. This complicates the design of precise transmit and receive frequency masks, leading to out-of-band emission issues. In addition, the extreme directionality required to close the link in this portion of the spectrum introduces a deafness problem which complicates the design of sensing- and beaconing-based sharing even when compared to mmWave frequencies.

B. Contributions and Paper Structure

The implementation of spectrum sharing techniques, therefore, requires a concerted effort involving the different stakeholders of the spectrum above 100 GHz, and innovations in both spectrum policy and engineering. This paper represents a critical step to make this portion of spectrum ready for the technologies that will use it in the future, replacing a set of regulations that date back to the 1930s [29], [30].

This paper provides policy and technological guidance on how sharing can be effectively implemented for the benefit of all the stakeholders in the spectrum above 100 GHz, enabling the digital revolution of the next decade. Notably, it is the first paper that:

- 1) describes the needs of the stakeholders in the spectrum above 100 GHz, detailing—with numerical examples—why both sensing and communications can benefit from access to large, contiguous chunks of bandwidth in this portion of the spectrum;
- 2) provides a detailed description of the current spectrum regulations in this band, highlighting possible policy roadblocks that prevent dynamic spectrum sharing between different stakeholders;
- 3) adopts a physics-based approach to model the interference between active systems and passive users, to understand which scenarios and operating regimes are

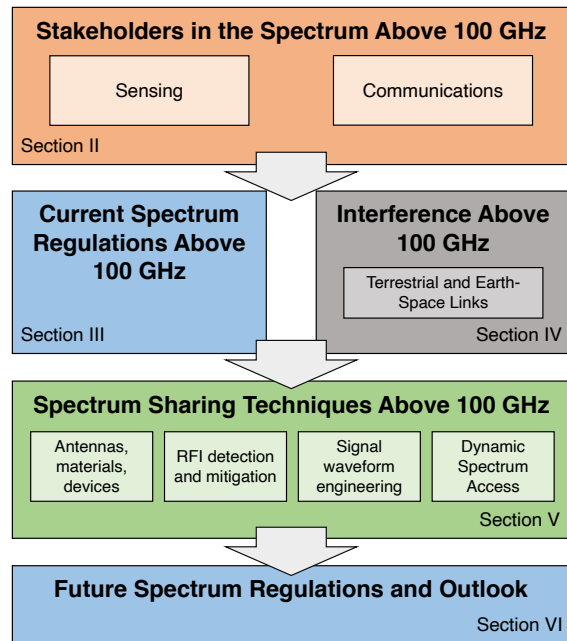


Figure 2: Structure of the paper

subject to RFI in the spectrum above 100 GHz. The modeling will consider realistic settings and conditions, i.e., high-sensitivity receivers for the sensing systems, and directional antenna arrays in the communication systems, and will be based on ITU channel models and antenna patterns. Our analysis highlights that while the high path loss and directional antennas can help reduce RFI in some scenarios, there are configurations (e.g., for high satellite elevation angles) where RFI from terrestrial communications links exceeds the harmful RFI thresholds for passive services set by the ITU;

- 4) analyzes technological enablers of spectrum sharing in the spectrum above 100 GHz, considering established techniques (e.g., signal processing for RFI mitigation), specific solutions at higher frequencies (e.g., metasurfaces and extremely directional arrays), and research directions and challenges toward spectrum sharing above 100 GHz. We review full-stack solutions, i.e., hardware-based RFI mitigation (innovative antenna design, antenna arrays, Frequency Selective Surfaces (FSSs)), signal processing, and communications and networking design;
- 5) discusses how spectrum regulations and technologies can evolve to accommodate more shared spectrum, proposing a future directions for technology and policy development, experimentation, and commercialization of sensing and communications solutions above 100 GHz.

The remainder of this paper is organized as follows (see Figure 2). Section II describes why the spectrum above 100 GHz is of interest for both the sensing and communication communities, and why more bandwidth is generally useful for both. Section III outlines the current regulations that prevent a flexible use of the spectrum above 100 GHz, while Section IV presents numerical results on the interference that can arise

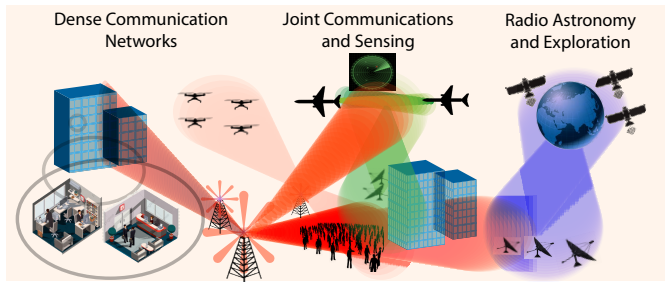


Figure 3: Stakeholders in the above 100 GHz band.

in different scenarios. Based on this analysis, Section V introduces and reviews possible spectrum sharing techniques and related research challenges. Finally, Section VI concludes the paper with a discussion on what is required to enable spectrum sharing above 100 GHz.

II. STAKEHOLDERS IN THE SPECTRUM ABOVE 100 GHz

As shown in Figure 3, the spectrum above 100 GHz is an attractive resource for a diverse set of stakeholders. In the following paragraphs, we will discuss why each user of the spectrum is interested in using a large bandwidth, focusing specifically on the spectrum above 100 GHz and providing a quantitative assessment when relevant.

A. Sensing

Sensing applications which require access to spectrum consist of three broad categories: radar systems, passive Earth-observing systems, and astronomy systems. Broadband (or continuum) and narrow-band applications are both important in the Earth-observing and astronomical contexts.

The narrow-band work focuses on detection of specific molecules. Key molecules for atmospheric science include molecular oxygen (at 60 GHz) and water vapor (at 183 GHz). For astronomy, the most important molecule has traditionally been carbon monoxide (CO) (at 115, 230 and 346 GHz), which is the most abundant asymmetric molecule, and hence the strongest emission feature from regions with dense gas.

Broad bandwidths can be desirable for molecular line astronomy. This is because of Doppler motions and general relativistic effects, due to the expansion of the Universe, which can have a significant impact by moving the sensing target out of typical narrow bands. With facilities that exist or are planned for the near future, the strongest molecular features may be detectable up to distances sufficiently close to the edge of the observable Universe. In this case, their wavelengths may be a factor of about 4 larger as we observe them than the wavelengths of the same molecular transitions as measured in a laboratory. This makes the case for a broadband access to the spectrum for radio astronomy sensing. Additionally, the increasing sensing capabilities of modern scientific facilities have allowed observers in recent years to measure phenomena related to a much larger number of rare molecules, which span the whole electromagnetic spectrum. In general, projects which involve characterization of the emission of a single known molecule can usually do well with narrow-band

observations, while projects which involve searches for new molecules typically need broadband access to the spectrum, even if the features to be observed are narrow ones.

Typical spectral widths of the features vary by application. Atmospheric features are susceptible to pressure broadening (i.e., the intrinsic energies of the transitions in one molecule can be affected by forces exerted from other molecules), and sometimes Zeeman broadening (i.e., they are broadened by forces from the Earth's magnetic field affecting the energy levels within molecules). Additionally, some atmospheric molecular features come in bands with many adjacent transitions. The oxygen absorption band, for example, consists of a large set of absorption features, pressure broadened to create a smooth feature from about 50-70 GHz, and the water vapor band at 183 GHz also spans a fairly broad range, dominating atmospheric opacity from about 165 GHz to 200 GHz [31]. Astronomical narrow-band features typically have widths no more than those of the Doppler shifts associated with the orbital speeds of galaxies. These are typically ≈ 200 -400 km/sec, giving fractional widths of about 1/1000, or a few hundred MHz. There are, however, also often isotopic features adjacent to the primary molecular feature that astronomers wish to observe simultaneously with the primary feature. These have fractional separations about the same as the fractional mass difference between the dominant and rarer isotopes, so they are typically shifted by about 5% from the main feature for the light molecules that are most abundant (e.g., in addition to CO at 230 GHz, there are ^{13}CO at 220 GHz and C^{18}O at 210 GHz).

Finally, broadband passive work also focuses on detection of thermal and synchrotron emission.¹ Broadband active sensing work largely involves the use of the millimeter band to do the same kind of work as lower frequency radars, taking advantage of the short wavelength at these frequencies to perform finer imaging. Broadband passive systems generally study phenomena with emission across the entire millimeter band, so the restrictions of sensing applications arise from the limitations on the receivers and the electronics and computational processing systems. Currently, these generally impose 20% fractional bandwidths on the receivers, and 8-50 GHz total bandwidth from the electronics. Nonetheless, technological improvements have consistently pushed these limits over the past few decades, and there are no indications that such progress is slowing down. The spectrum above 100 GHz is also used for some very short range imaging applications (e.g. medical imaging and security scanners).

In the following paragraphs, we will discuss in details use cases for narrow-band and continuum sensing.

Narrow-band applications. The narrow-band applications are largely driven by a particular set of frequencies for specific rotational transitions of molecules, largely within the 10-500 GHz range. Earth-sensing satellites and high altitude airplanes can use these molecular features to map out quantities such as chemical composition of the atmosphere and cloud cover and humidity, among others [32]–[34]. Such

¹Synchrotron emission is the relativistic version of cyclotron emission, and is produced when electrons with speeds very close to the speed of light produce radiation as they are accelerated by magnetic fields.

measurements are important for both meteorology and climate science.

For astronomical objects, molecular features can provide information not just about chemical compositions, but also temperatures and densities of regions in space. Temperatures are largely probed by the fraction of a single compound's molecules in different excited states, while densities and chemical compositions can then be inferred from the relative abundances of different molecules. In recent years, improvements in the sensitivity of astronomical facilities in the 10-500 GHz band have made it possible for astronomers to detect a wide range of new molecules [35]. The newest facilities can also detect molecules with the brightest features at distances where the expansion of the Universe introduces large cosmological redshifts [36]; these large cosmological redshifts can also move important molecular transitions out of protected bands, into unallocated frequency ranges. Both of these developments mean that even the portion of the passive sensing community working with narrow spectral features has *applications that span the full spectrum*.

Broadband (or continuum) sensing. There is considerable interest in moving automotive and other radar systems above 100 GHz, although this work is still in relatively early stages of development [37], [38], as the larger bandwidth and shorter wavelength lead to better range, angular and velocity resolutions. The range resolution ΔR of a radar based on pulse compression depends on the bandwidth of the transmitted pulse, i.e.,

$$\Delta R = \frac{c}{2B}, \quad (1)$$

where c is the speed of light and B is the bandwidth. The angular resolution depends on the antenna beamwidth, which is related to the electrical length and corresponding directivity of the antenna. The velocity resolution depends on the Doppler spectrum that is also related to the wavelength of the transmitted signal. Moreover, in some cases, the propagation challenges of working in the above 100 GHz band are a positive feature; a higher density of automotive radar systems can be tolerated if propagation losses keep the systems from interfering with one another over large distances.

Broadly speaking, however, the continuum work presently done in this band is radio astronomy. Continuum work in radio astronomy is usually done to look at cool thermal emitters, such as (i) interstellar dust; (ii) the disks around young stellar objects, in which planets form (which typically have temperatures of a few hundred Kelvin); or (iii) the cosmic microwave background (which has a temperature of 2.7 K). It can also be used to look at sources of synchrotron emission at high frequencies. The highest angular resolution images that can be made by astronomers come from millimeter-band very long baseline interferometry, work done at 230 GHz [39]. At longer wavelengths, the angular resolution is insufficient to measure black hole shadows without space-based antennas (which currently lack the sensitivity to do so). At infrared bands, interferometry has only been possible with direct interference of signals from physically connected telescopes, limiting baselines to a few hundred meters. The millimeter band is the shortest wavelength on which data

can be recorded and global baselines can be achieved. This capability allowed—for example—the measurement of the size of the shadow of a black hole event horizon in the galaxy M87 [39]. In most cases of continuum imaging, the largest possible bandwidth is desired in order to detect faint signals, but for sufficiently bright sources, with sufficiently large bandwidths, the spectral shape of a source can be measured with a single observation at a single band.

The sensitivity of a radiometer is derived from the radiometer equation:

$$\Delta T = \frac{T_{\text{sys}}}{\sqrt{B\tau}}, \quad (2)$$

where ΔT is the residual (root-mean-square) uncertainty in a noise temperature measurement, T_{sys} is the noise temperature of the system being measured, and $B\tau$ is the product between bandwidth B and time τ of observation [40]. The signal-to-noise of a source is then derived from the ratio of the source brightness temperature, T_{source} , and ΔT . Notably, $T_{\text{source}} = \left(\frac{A_e}{2k_B}\right) S_\nu$, where A_e is the effective area of the system, k_B is the Boltzmann constant and S_ν is the flux density of the source per angular resolution element.

Radio astronomy requires ultra-low noise levels. Reaching these in short exposure times is always desirable, as, at a minimum, it enables a larger number of observations to be done. Additionally, in some cases, strong source variability is the goal of the measurement itself [41], with the consequence that the measurement must be completed quickly in order to make reliable aperture synthesis images [39]. Increases in sensitivity in a given exposure time can be achieved either by increasing the bandwidth available or by increasing the effective area of the system. Bandwidth increases are generally preferred because electronics upgrades are usually much less expensive than adding antennas or increasing the sizes of the antennas used. Available bandwidth currently varies among the different telescopes. The receiver bands are generally limited to about 20% of the central frequency. At the present time, millimeter band interferometers typically use about 8 GHz, with the specific frequencies chosen based on the science case for the user.^{2,3} However, for the Atacama Large Millimeter Array, planning is already underway to upgrade the correlators to allow at least a factor of 2 increase in bandwidth [42]. Single dish radio telescopes have larger bandwidths; for example, the TolTEC instrument for the Large Millimeter Telescope planned to reach about 60 GHz of bandwidth.⁴ The present regulatory framework was established in an era long before the current tens of GHz of bandwidth systems were practical.

Currently, a rather limited number of radio astronomy facilities engage in sensing above 100 GHz. All such facilities are in high altitude, dry locations, generally several kilometers or more from settled locations; the requirement of detecting faint signals mandates choosing sites with minimal propagation losses. A substantially larger (albeit still small) number of telescopes work in the 90 GHz band, and the CLOUDSAT satellites of NASA have successfully avoided interfering with

²<https://almascience.eso.org/about-almal/almal-basics>

³<https://www.iram.fr/IRAMFR/GILDAS/doc/pdf/noema-intro.pdf>

⁴https://people.astro.umass.edu/wilson/TolTEC_website/about.html

them for 15 years. It should be straightforward to continue to avoid interference with ground-based scientific users.

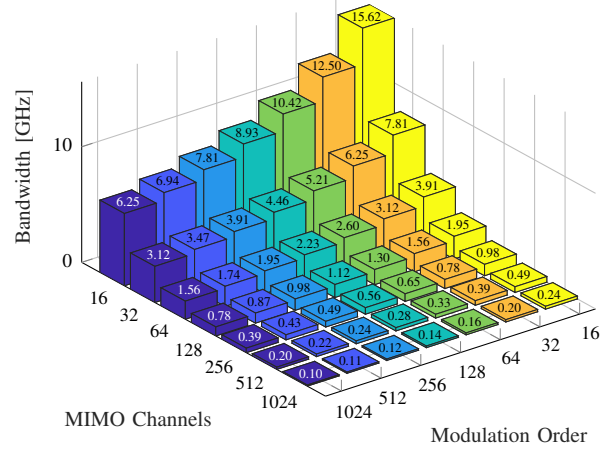
B. Communications

Several early papers on 6G communication technologies have highlighted how the spectrum above 100 GHz could be a fundamental enabler of ultra-high-capacity wireless networks [16], [27], [43]. Results and demonstration of the feasibility of communicating in the (sub) terahertz bands have also been shown in several works, for example as in [44]. The main challenges for communications in this portion of the spectrum are associated to (i) the sensitivity to blockage and the high propagation loss [11], which can be offset, however, using directional antennas; (ii) the presence of frequency selective fading in specific bands, which increases with the humidity; and (iii) the engineering and manufacturing of embedded RF circuitry that can operate at such high frequencies [45]. Additional challenges are related to the interfacing with the higher layers of communications protocol stacks, such neighbor and infrastructure discovery challenged by directional links, and processing data at ultra-high rates [16].

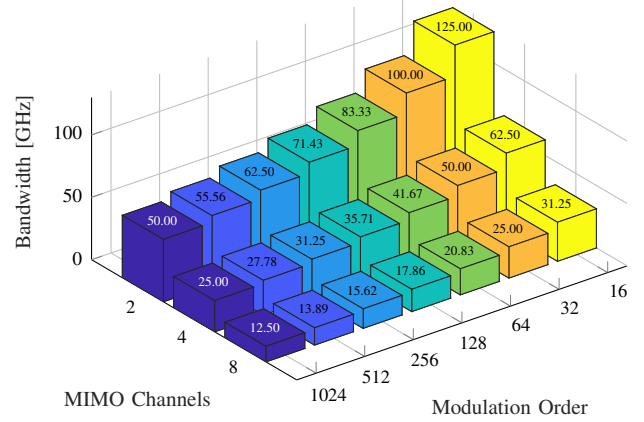
Nonetheless, the need for Tbps data rates in 6G networks makes a compelling use for the deployment of communication services in the spectrum above 100 GHz, with a vast available bandwidth. Indeed, the achievable data rates R of a wireless link (with an ideal, frequency-flat channel) is proportional to the bandwidth B , scaled by the spatial reuse or diversity factor K and the spectral efficiency S , and by a function $f(\cdot)$ of the link Signal to Interference plus Noise Ratio (SINR) Γ :

$$R \propto K \cdot S \cdot B \cdot f(\Gamma). \quad (3)$$

Here, $f(\cdot)$ is a generic function expressing the relationship between SINR and achievable rate, and the different elements K, S, B in Eq. (3) highlight how next-generation communication technologies can improve on existing ones to increase the communication rates. Notably, a higher spectral efficiency can be achieved through more spectrally-efficient modulations, e.g., Orthogonal Frequency Division Multiplexing (OFDM) and its variants [46]–[48], combined with high order Quadrature Amplitude Modulation (QAM) (with 1024-QAM and even above). This is represented in Eq. (3) by the scaling factor $S = \log_2(M)$, with M the modulation order. Spatial reuse and diversity can be achieved using Multiple Input, Multiple Output (MIMO) techniques, which allow multiple data streams to be transmitted over the same time and frequency resources. This is represented in Eq. (3) by the scaling factor K , which we model as the number of MIMO streams, proportional to the rank of the channel matrix. A recent MIMO evolution, i.e., massive MIMO [49], has been shown to improve the SINR term as well, by exploiting the much larger number of antennas at the transmitter as compared to the receiver. The idea of Ultra Massive MIMO (MIMO) [50] extends this even further, by packing thousands of antenna elements in small, portable arrays. Small cells and ultra-dense networks also help increase the spatial reuse factor K , sometimes at the cost of increased interference which penalizes the term Γ . Similarly, increasing the communication bandwidth B allows for a linear increase



(a) High number of MIMO streams (e.g., enabled by massive MIMO).



(b) Low number of MIMO streams.

Figure 4: Required bandwidth to achieve a 1 Tbps data rate, as a function of modulation order and MIMO channels for OFDM.

in the product outside function $f(\cdot)$, but at the same time, the noise term of the SINR Γ increases proportionally to B .

The data rate increase for 6G networks will be given by a combination of the elements above. Nonetheless, the bandwidth plays a key role, as we show in Figure 4. Each bar in the figure represents the bandwidth required to achieve a data rate of $R_t = 1$ Tbps, which is expected to be one of the defining Key Performance Indicators (KPIs) of 6G networks [15], [51] for a number of applications, including backhaul [51]–[53], immersive, holograph-based virtual experience [54], data offloading in vehicular networks [55], and mobile hotspot scenarios [51]. Notably, the bandwidth is computed as the ratio between the target rate R_t and the efficiency η of the MIMO and modulation order in use, i.e., $\eta = \hat{K} \hat{S} / \alpha$, with \hat{K} the number of MIMO streams, \hat{S} the bit per symbol rate of a certain modulation order, and $\alpha = 1$ for single-sided waveforms, 2 otherwise. Figure 4a considers a configuration with massive MIMO capabilities, and highlights how an extremely high number of MIMO channels, combined with a high modulation order, makes it possible—in principle—to reach the data rate target with bandwidths that are comparable to those of current 5G systems. Designing and engineering a system with such capabilities, however, is not trivial. A large number of MIMO

Band (GHz)	122.25-130	158.5-164	167-174.8	191.8-200	231.5-235	238-241
Bandwidth (GHz)	7.5	5.5	7.8	8.2	3.5	3
Primary allocation	Fixed-Satellite/Mobile-Satellite	Fixed/Mobile	Fixed/Mobile	Fixed/Mobile	Fixed/Mobile	Fixed/Mobile

Table I: Bands above 100 GHz with Mobile or Fixed allocations without passive allocations. Most of these bands have co-primary allocations with other active services.

streams requires a massive number of antennas, as well as diversity in the channel conditions, and this may not be always feasible, especially when considering point-to-point backhaul links or portable devices in the sub-6 GHz spectrum.

Portable arrays with hundreds of antenna elements are instead feasible above 100 GHz, thanks to the small wavelength which translates into small antenna elements [50]. At such high frequencies, however, it becomes extremely complex to design multi-channel and/or multi-user MIMO systems with a high number of channels. The state of the art of the research on baseband design for such systems is represented by 4x4 and 8x8 MIMO systems [56], [57]. To this end, Figure 4b considers configuration with a more practical number of parallel MIMO streams (i.e., up to 8). In this case, even with an OFDM modulation with 1024 QAM per channel, more than 12.5 GHz of contiguous bandwidth are needed.

Additionally, such constellations often require extremely good channel conditions and low noise (both in amplitude and phase). Therefore, more practical configurations are represented on the right part of Figure 4b, with 16 QAM, which further increases the requirement in terms of bandwidth (i.e., 31.25 GHz with 16 QAM and 8x8 MIMO). Therefore, *the need for ultra-wide bandwidth makes the spectrum above 100 GHz a key enabler for future 6G communications.*

III. CURRENT SPECTRUM REGULATIONS ABOVE 100 GHz

Enabling sharing of the spectrum above 100 GHz will require both technological progress and policy updates. This section reviews the development of spectrum policy for the bands between 100 GHz and 275 GHz (as there are no formal ITU allocations above 275 GHz yet), highlighting the roadblocks and opportunities towards a sharing-conscious spectrum policy. Notably, we review and summarize international regulations and provide an historical perspective on how they have been developed, together with a discussion on how the characteristics of the spectrum above 100 GHz have led to different policies when compared to sub-6 GHz or lower mmWave spectrum.

A. International Telecommunications Union (ITU)

At the international level, the spectrum is regulated by the ITU, a United Nations agency with 193 Member states that develops the ITU Radio Regulations (RR), a treaty document generally binding on its signatories. While these rules do not require countries to use spectrum in certain ways, they prohibit them from causing “harmful interference” to spectrum uses of other countries which are fully consistent with the rules. While most regulations involve active transmitters for applications such as telecommunications, broadcasting and radar/radiolocation, the ITU also recognizes and protects passive scientific uses of the spectrum. As discussed in Section II,

these use cases involve only the reception of naturally occurring emissions in specific spectrum bands, for example for radio astronomy and environmental monitoring. Notably, the spectrum above 100 GHz features several bands which are reserved for the passive community. Table I and Figure 1 list the bands with primary or co-primary Fixed and/or Mobile allocations, without any co-primary passive allocation:⁵ in the present allocation scheme, the maximum fixed or mobile congruous bandwidth below 252 GHz is 8.2 GHz. This, as previously discussed, motivates the development of spectrum sharing solutions.

B. WRC-2000 and spectrum policy above 100 GHz

Prior to the ITU WRC in 2000, ITU had few rules and allocations dealing with spectrum above 100 GHz. At that conference, similar proposals from both the United States and the European Conference of Postal and Telecommunications Administrations (CEPT) advocated the basic policies now in place in 100-275 GHz [58]. The policies advocated by the US and Europe included both numerous passive allocations above 100 GHz, some bands with no passive allocations at all, and some bands in which active services and passive services could nominally share on a “co-primary” basis.

Ten passive-only bands were created in the 100-275 GHz spectrum, using the restriction in footnote 5.340 of the Allocation Table (also known as RR5.340) [18], previously used for lower frequency passive bands. RR5.340 states that “all emissions are prohibited” in these bands, which cover 19% of the 100-275 GHz spectrum. Table II compares the amount of “prohibited” spectrum in the Extremely High Frequencies (EHF) band (30-300 GHz) with lower spectrum regions. While the amount of prohibited spectrum in Ultra High Frequencies (UHF) and Super High Frequencies (SHF) (below 30 GHz) is negligible, it covers 15% of the entire EHF region. In addition, the 15 protected bands in the EHF spectrum fragment the band allocations in ways unknown in lower regions. Finally, these passive allocations are more dense in the 100 GHz region, because molecular resonances that are of interest to astronomers and environmental scientists are more densely concentrated above 100 GHz than below [22].

WRC-2000 and succeeding conferences have defined 18 bands with co-primary passive allocations above 100 GHz. In some, passive allocations are co-primary with terrestrial fixed and mobile services, and in some others, only with other services, including inter-satellite links. These co-primary bands cover 58% of the spectrum in this region. As a result,

⁵Primary users are the only entities that can legitimately use a portion of the spectrum and are entitled to protection from harmful RFI from secondary users. In case of multiple co-primary allocations, the co-primary users need to coordinate with each other to avoid harmful RFI.

Band	Frequency (GHz)	Number of RR5.340 Passive Blocks	Fraction of Band Passive
UHF	0.3–3	2	1%
SHF	3–30	3	2%
EHF	30–300	15	15%

Table II: Prohibited bands according to RR5.340 in different spectrum regions.

77% of the spectrum in 100-275 GHz has either primary of co-primary passive allocations.

ITU regulations define 3 basic types of passive services with such allocations, that broadly classify the spectrum stakeholders described in Section II: Radio Astronomy Service (RAS), Earth-Exploration Satellite Service (EESS), and Space-Exploration Service (SES). RAS is the oldest, and involves Earth-based sensors looking radio sources from sources far away from the Earth. In practice at frequencies above 100 GHz atmospheric absorption of such signals is a major issue so the best locations are high altitude arid sites. In particular, Chile’s Atacama Desert is a major location for such observatories. There are few observatories in the spectrum in US territory and the only one near a US urbanized area is the Arizona Radio Observatory at Kitt Peak about 80 km from Tucson AZ. Traditionally, RAS observatories have been protected from active users of the same bands by coordinating the siting and parameters of transmitter within an established “coordination zone” [59]. National spectrum regulators establish zones around radio telescopes in which all transmitters need prior discussion with the radio telescope operators before they can be installed. The size of these coordination zones depends on both the frequencies being used at the radio telescope and the specific terrain around it. Indeed, RAS antennas point upward and thus can only receive power from terrestrial transmitters that are in or near a line of sight from the antenna, therefore assessing transmitter locations, direction, and power levels in coordination areas is of utmost importance. Table III summarizes the allocations with RAS as the co-primary user for Fixed/Mobile users, which already potentially represent a first option for spectrum sharing with terrestrial active users. Finally, an emerging source of possible RFI for RAS antennas is represented by aerial vehicles, e.g., airplanes or Unmanned Aerial Vehicles (UAVs), that maintain connectivity with the ground.

Differently from RAS systems, EESS antennas are on non-geostationary satellites at orbit heights of 400-800 km and point towards a large area on the Earth, although some limb sensing antennas point towards the horizon. EESS satellite makes observations throughout their orbits and thus could be affected by sidelobe or scattered power from terrestrial radio systems in their bands and thus are the most difficult class of passive systems to protect, both from regulation and technological standpoints.

The unusual density of passive bands above 100 GHz fragments the available spectrum, forbidding or complicating the use of large contiguous bandwidths. These condition currently hold in the 100-275 GHz band, as also shown in Figure 1:

- the largest bandwidth with a present fixed or mobile allocation but no co-primary passive allocation is 8.2 GHz

(191.8-200 GHz);

- the largest contiguous bandwidth possible for active use (but not necessarily fixed or mobile allocations) without overlapping a RR5.340 band is 32.5 GHz (116-148.5 GHz); and
- the largest bandwidth for active use without overlapping any band with a EESS allocation is 26.25 GHz (122.25-148.5 GHz).

Thus use of bandwidth greater than 26.25 GHz for active use will require sharing with a primary or co-primary passive service, motivating the development of technological solutions for active/passive spectrum sharing. To extend active uses to 32.5 GHz, active and passive users will need to share RR5.340 bands. Doing so will not only require technological innovations, but also the development of new policies. An apt starting point for such policies would be research findings which indicate bands less likely to be subjected to interference, and be ratified by ITU-R. The process involves placing the issue in an agenda at a WRC conference, followed by discussion and, (in case) approval at the next WRC conference. It is worth noting that WRC conferences happen every four years, which reduces the speed of the overall process.

C. ITU-R Resolution 731 and Spectrum Sharing Policy

At WRC-2000, the US and CEPT proposals also included a provision to study whether sharing of the allocated passive bands with active services was possible without harmful interference. In 2000, on the eve of the commercial introduction of 3G / Universal Mobile Telecommunications System (UMTS) cellular technology, such studies were complicated by the fact that there were few indications of what meaningful telecommunications applications above 100 GHz, or even what data rates would be required in the long term, for either mobile links or the backhaul. Resolution 731 [26] was approved as a compromise between the suggested language of the US and CEPT on spectrum sharing. It states that ITU-R should study possible sharing of the passive bands above 71 GHz with other spectrum uses, and that such sharing must not expose the passive service to interference levels greater than those specified by ITU-R recommendations [23]–[25]. At WRC-19, Resolution 731 was then updated to add new provisions for above 275 GHz, but its provisions within the 71-275 GHz spectrum remained the same, except for updating references to other ITU-R documents.

Resolution 731 specifies explicit interference criteria for EESS [23] and for RAS [24], [25]. In the case of EESS, the criteria given is a triplet of numbers for each protected band which specifies: (i) the reference bandwidth over which interference power should be measured; (ii) the maximum permitted interference level; and (iii) the percentage of the Earth’s surface area or time in which the permissible interference level may be exceeded. These power levels are defined at the terminals of the receiving antenna in the satellite. They represent the total power received from the area of the Earth that is viewed by the antenna’s footprint, including its sidelobes. A separate ITU-R document [60] gives typical satellite parameters, such as orbit height and antenna characteristics but does not presently cover every possible band

Band (GHz)	102-109.5	111.8-114.5	141-148.5.8	151-155.5	155.5-158.5	209-226	252-265
Bandwidth (GHz)	7.5	2.45	7.5	4.5	3.5	3	13
Active co-primary allocation				Fixed/Mobile			
Passive co-primary allocation	RAS	RAS	RAS	RAS	RAS, EESS	RAS	RAS

Table III: Bands above 100 GHz with Mobile or Fixed allocations with RAS co-primary passive allocations.

(although an update is in progress [61]). The analysis of the available literature on EESS, however, does not exhaustively clarify if all passive satellites have interference vulnerability comparable to that specified in this document. It is also not clear whether there is public information available on all passive satellites entitled to interference protection and their parameters, including orbit parameters.

Finally, Resolution 731 also contains the following provision: “to the extent practicable, the burden of sharing among active and passive services should be equitably distributed among the services to which allocations are made” [26]. This implies that, when developing sharing strategies, both the active and passive users have an obligation to cooperate to increase the overall use of the spectrum, while also achieving the user-specific objectives. Nonetheless, passive satellite systems do not have the same level of flexibility as active users. The design of satellites and scientific equipment is a multi-year effort, and careful planning needs to be factored in the engineering of the RF components. Once in orbit, there is little or no possibility to change operating parameters and adjust transceiver systems to react to new or unforeseen interfering signals. As of today, most passive satellites orbiting are expensive units, with a mission lifetime spanning 5 to 15 years. It is also difficult to change parameters for satellites that are planned but not launched yet, even if consensus on the policy and sharing technologies is reached. So far, there has been no ITU-R discussion on the concept of “burden sharing” as introduced in Resolution 731, even though this holds long term potential for improving spectrum sharing capability.

IV. INTERFERENCE ABOVE 100 GHz: LINK BUDGET ANALYSIS

As discussed in Section III, there exist some bands in which the active users are forbidden from emitting any RF signals. Herein, we present numerical results that highlight scenarios in which harmful interference arises, and deployments in which the same is rendered void. We first describe our modeling approach (Section IV-A), based on ITU channel models, and then the results (Sections IV-B and IV-C). Notably, we analyze terrestrial and aerial links as they represent typical communication and interference scenarios, e.g., with a backhaul link on the ground generating RFI toward a satellite.

A. System Model

We consider the system model shown in Figure 5: a terrestrial link between two ground stations (e.g., a terrestrial backhaul link [16], [62]), potentially interfering with a satellite orbiting over the terrestrial deployment area. The ground stations are equipped with directional antennas and can use multiple digital modulations, bandwidths, and carrier frequencies, as shown in Table IV.

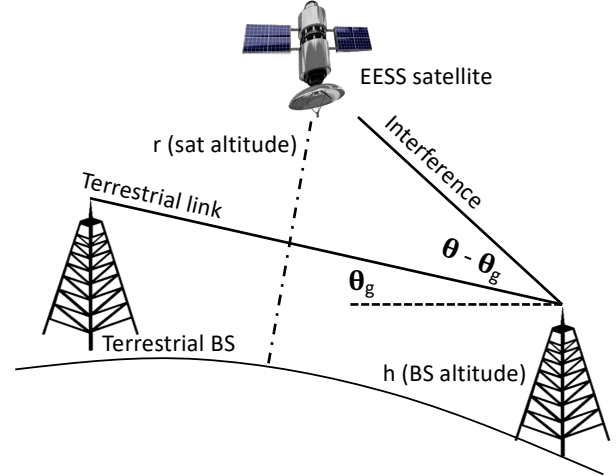


Figure 5: System model

For the terrestrial link, the received power $P_{rx,g}(f, d)$ (in dB) can be expressed as a function of the distance d and the carrier frequency f :

$$P_{rx,g}(f, d) = P_{tx,g} - L(f, d) + G_{g,tx,max} + G_{g,rx,max}, \quad (4)$$

where $P_{tx,g}$ is the transmit power of the ground transmitter, L is the path loss for a terrestrial link, and G is the antenna gain. We assume, without loss of generality, that the transmitter and receiver are aligned and experience the maximum antenna gain.

For the Earth-space link, the received power at the satellite, as a result of the interference from the ground station, can be expressed as (in dB)

$$P_{rx,s}(f, d, \theta, \theta_g) = P_{tx,g} - L(f, d) + G_{tx}(\theta - \theta_g) + G_{sat}(\theta - \theta_g), \quad (5)$$

where L is the path loss for an Earth-space link, G is the antenna gain, θ_g is the tilt of the ground transmitter antenna, and θ is the elevation angle between the ground transmitter and the satellite, as shown in Figure 5.

We model the terrestrial and Earth-space path loss using ITU path loss models [63]–[66], which include the conventional free-space path losses or spreading losses and the molecular absorption losses. These models are generally considered for the development of ITU recommendations, and show consistency with other methods (e.g., based on the HITRAN database [11]) in the frequency range of interest (even though they diverge at higher frequencies) [67]. The free-space attenuation L_{spr} is due to the expansion of the wave as it propagates through the space and is calculated (in dB) as [63]

$$L_{spr}(f, d) = 92.45 + \log(fd), \quad (6)$$

Parameter	Value
Channel model	Based on ITU-R [63]–[66]
Antenna gain model	Based on ITU-R [69]
$G_{g,i,\max}, i \in \{\text{tx}, \text{rx}\}$	40 dBi
G_{sat}	{20, 40} dBi
$P_{\text{tx,g}}$	{18.6, 33.4} dBW (see Section IV-C)
f_c	{150, 183, 230} GHz
Noise PSD	$N_0 = -160$ dBW
Modulation	16-QAM, 64-QAM, 256-QAM, 1024-QAM
Bandwidth	Based on Figure 4

Table IV: System parameters.

where f is the frequency of the signal in GHz, and d is the propagation distance in km. For Earth-space slant paths, this distance is

$$d = \sqrt{R^2 \sin^2 \theta + 2Rr + r^2} - R \sin \theta, \quad (7)$$

where r is the satellite altitude, θ is the elevation angle and R is the Earth radius [68].

The molecular absorption losses are due to the interaction of the RF signal with air molecules. As mentioned in Section II-A, certain frequencies of interest result in the greater resonance with specific molecules, leading to a frequency dependent absorption loss. At frequencies above 100 GHz, the main contributor to absorption loss is water vapor [11]. Thus, the specific gaseous attenuation at height h is given by $\gamma(h) = \gamma_o(h) + \gamma_w(h)$ (dB/km), where $\gamma_o(h)$ and $\gamma_w(h)$ are the specific attenuation due to dry air and water vapor, respectively [64]. Due to the inherent frequency selective and medium dependent nature of absorption losses, it is dependent both on the frequency of the RF signal, and the characteristics of the medium through which the signal travels (such as temperature, pressure and humidity, and density). For different Earth-space slant paths, the signal traverses different atmospheric heights, which lead to different temperatures and pressures [65]. Taking into account these factors, the total absorption loss L_{abs} is then calculated as

$$L_{\text{abs}} = \int_0^r \frac{\gamma(h)}{\sqrt{1 - \cos^2 \theta(h)}} dh, \quad (8)$$

where $\gamma(h)$ is the specific gaseous attenuation at height h and $\theta(h)$ is the local apparent elevation angle at height h , which depends on the refractive index at that height [66]. Combining these, the total path loss is then

$$L = L_{\text{spr}} + L_{\text{abs}}. \quad (9)$$

The antenna gain model also follows ITU recommendations. Notably, we consider the model in [69] for above 70 GHz, which models the gain as a function of the off-axis angle θ , the carrier frequency f_c , and the maximum gain G_{max} (in dB). The ITU model first computes the antenna diameter D as a function of G_{max} as

$$D \approx \lambda \cdot 10^{\frac{G_{\text{max}} - 7.7}{20}}, \quad (10)$$

where $\lambda = c/f_c$ is the wavelength. Then, it defines the first-lobe gain G_1 as

$$G_1 = 2 + 15 \log_{10} \left(\frac{D}{\lambda} \right). \quad (11)$$

In the case of $D/\lambda > 100$, the gain G as a function of the angle θ is computed as

$$G(\theta) = \begin{cases} G_{\text{max}} - 2.5 \cdot 10^{-3} \left(\frac{D}{\lambda} \theta \right)^2, & 0 \leq \theta < \theta_m \\ G_1, & \theta_m \leq \theta < \theta_r \\ 32 - 25 \log_{10}(\theta), & \theta_r \leq \theta < 120^\circ \\ -20, & 120^\circ \leq \theta < 180^\circ, \end{cases} \quad (12)$$

where

$$\theta_r = 15.85 \left(\frac{D}{\lambda} \right)^{-0.6}, \quad (13)$$

and

$$\theta_m = \frac{20D}{\lambda} \sqrt{G_{\text{max}} - G_1}. \quad (14)$$

If $D/\lambda \leq 100$, instead, the gain is

$$G(\theta) = \begin{cases} G_{\text{max}} - 2.5 \cdot 10^{-3} \left(\frac{D}{\lambda} \theta \right)^2, & 0 \leq \theta < \theta_m \\ G_1, & \theta_m \leq \theta < 100 \frac{\lambda}{D} \\ 52 - 10 \log_{10} \left(\frac{D}{\lambda} \theta \right) - 25 \log_{10}(\theta), & 100 \frac{\lambda}{D} \leq \theta < 120^\circ \\ -10 \log_{10} \left(\frac{D}{\lambda} \theta \right), & 120^\circ \leq \theta < 180^\circ. \end{cases} \quad (15)$$

The Signal-to-Noise-Ratio (SNR) $\Gamma = P_{\text{rx},i}/(N_0B)$, $i \in \{\text{g}, \text{s}\}$ is computed using a noise Power Spectral Density (PSD) $N_0 = -160$ dBW. Here, we consider a noise model based on empirical measurements on the receivers in the TeraNova platform [70], where the electronic noise temperature of the system dominates the noise temperature due to molecular absorption and the overall amplitude noise follows a Gaussian distribution. For B , we consider the bandwidth that is required to achieve a 1 Tbps data rate with a certain modulation and coding scheme, as shown in Figs. 4a and 4b (Section II). We then utilize the SNR to estimate the error rate probability for specific digital modulation and coding rates [71].

B. Path Loss Analysis

We first analyze the path loss for the terrestrial and Earth-space links.

1) *Terrestrial links*: Figure 6 shows the path loss at three different carrier frequencies, for a link between two ground stations at different altitudes. The path loss curves have a typical L-shaped trend, as the spreading loss increases logarithmically with the distance (thus linearly with respect to the logarithmic plots in Figure 6), while the absorption loss is linear with the distance (thus exponential in the plots of Figure 6). This can be seen also by comparing the path loss at different altitudes. At higher altitudes, the atmosphere is less dense; the absorption loss reduces accordingly. As shown in Figure 6, the path loss for $h = 10$ km maintains a logarithmic trend with the distance, while the L-shape is more evident for the path loss at $h = 0$ km. Finally, the path loss is similar for $f_c = 150$ GHz and for $f_c = 230$ GHz, with the latter having a slightly higher spreading loss. Instead, when considering $f_c = 183$ GHz (Figure 6b) the impact of the absorption is dominant, as this frequency corresponds with a water vapour absorption peak. The path loss due to absorption is again reduced at higher altitudes, due to a less dense atmosphere.

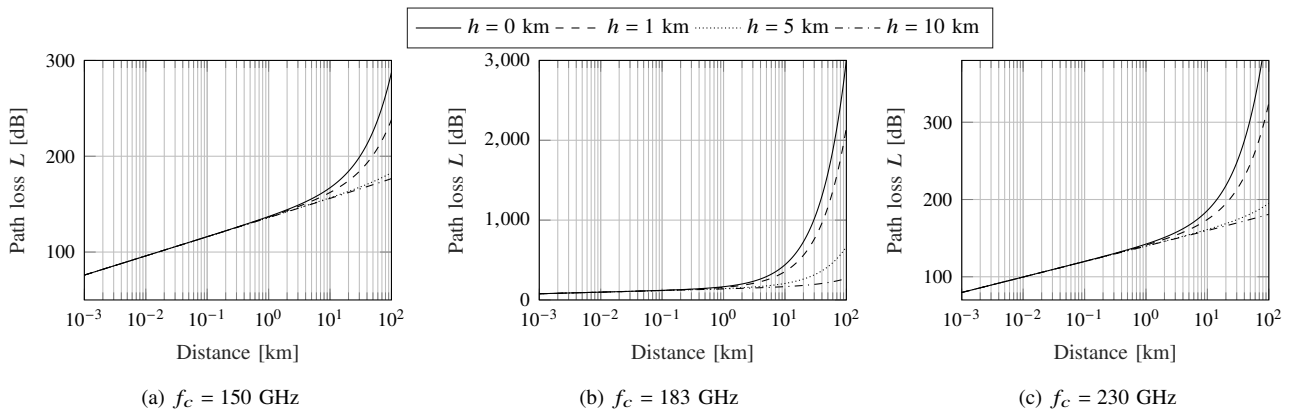


Figure 6: Path loss L as a function of traveled distance for terrestrial links and different altitudes h .

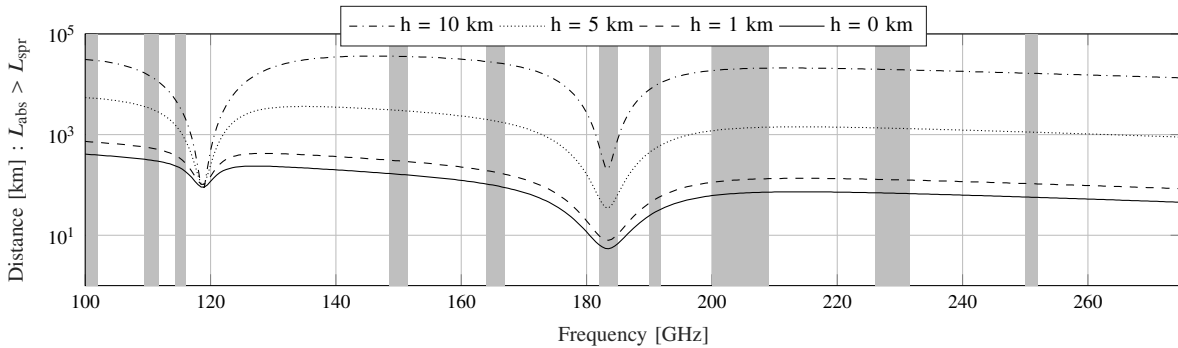


Figure 7: Distance at which $L_{\text{abs}} > L_{\text{spr}}$. The dark region correspond to RR5.340 bands.

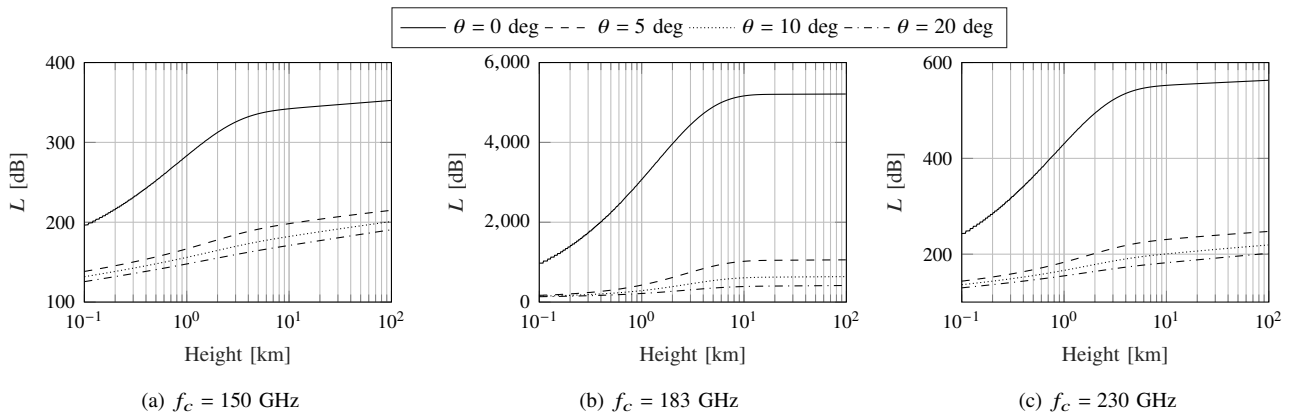


Figure 8: Earth-space path loss as a function of the satellite height, for different elevation angles θ .

To further investigate the interplay between spreading and absorption loss, Figure 7 reports the distances (in km) at which the absorption loss L_{abs} becomes larger than the spreading loss L_{spr} , for different frequencies and altitudes of the link. These results indicate that—outside absorption peaks—the contribution of L_{abs} is smaller than that of L_{spr} even for tens of km, even for the dense atmosphere at $h = 0$ km, demystifying the claim that communications in the above 100 GHz band are limited by the absorption phenomena.

2) *Earth-space Slant Paths*: The different composition and density of the Earth's atmosphere at different altitudes has an impact on the path loss trend for Earth-space paths. Figure 8 reports the path loss L for three different frequencies, as

a function of the satellite altitude and the elevation angle between the ground station and the satellite.

The curves exhibit a reverse L-shaped trend, especially for an elevation of 0 degrees. This shows that there exists two regimes for the path loss. Below a certain altitude threshold, which is at most 10 km for the elevation of 9 degrees and $f_c = 183$ GHz, the path loss is affected by the combined spreading and absorption losses. This leads to a much higher path loss for $f_c = 183$ GHz (Figure 8b) than $f_c = 150$ GHz and 230 GHz. Above this threshold, however, the less dense atmosphere leads to a reduced impact of the absorption loss L_{abs} , with the dominant contribution given by the spreading loss L_{spr} . This behavior is more evident for configurations

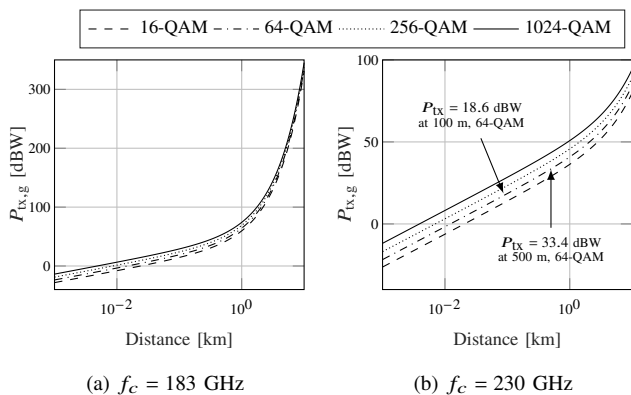


Figure 9: Transmit power $P_{tx,g}$ to achieve a 1 Tbps data rate with a bit error rate smaller than 10^{-5} , for different modulations and as a function of the distance between the terrestrial transmitter and receiver.

with the satellite at a lower elevation, as the signal has to travel through a thicker portion of the Earth atmosphere. The higher path loss for lower elevation angles is key to reducing interference from ground stations to satellites, as we discuss in Section IV-C.

C. Link Budget and RFI Analysis

To identify a meaningful transmit power value for the ground station in the interference analysis, we analyze the link budget for a terrestrial link that supports a data rate of 1 Tbps with a Bit Error Rate (BER) smaller than 10^{-5} . We consider the system model described in Section IV-A, with the parameters from Table IV, and the bandwidth for different modulations shown in Figure 4b.

Figure 9 reports the transmit power $P_{tx,g}$ that satisfies the required constraints for $f_c = 183$ GHz and $f_c = 230$ GHz, and four different QAM modulation orders. Considering that the number of MIMO streams supported by the link depends on the diversity of the physical channel and not on the wireless link design itself, we compute the target $P_{tx,g}$ by considering the average of the transmit power required with 2, 4, or 8 MIMO channels.

As expected, the impact of the higher absorption loss at 183 GHz translates into a higher required $P_{tx,g}$ than at 230 GHz, in particular for transmitter-receiver distances larger than 1 km. Additionally, high-order modulations need a higher $P_{tx,g}$ than low-order modulations, with an average 14.46 dB gap between 16-QAM and 1024-QAM. This disparity exists in spite of the reduced bandwidth requirements with high-order modulations to achieve the target rate of 1 Tbps.

In the following paragraphs, without loss of generality, we consider two arbitrary reference values for $P_{tx,g}$, i.e., $P_{tx,g} = 18.6$ dBW, which enables a data rate of 1 Tbps with 64-QAM at 100 m, and $P_{tx,g} = 33.4$ dBW, which corresponds to 1 Tbps data rate at 500 m, again with 64-QAM. These distances are typical representations of a backhaul link in a dense, urban environment. While we acknowledge that such transmit power levels (i.e., 72 W and 2.18 kW) are not feasible at the moment in above-100-GHz devices, they allow us to speculate on interference levels that orbiting satellites may experience in a typical 6G deployment. Similar values are

Band [GHz]	Maximum Interference Level [dBW]	Lowest Satellite Altitude [km]
115.25-122.25	-166 (N), -189 (L)	705 Aura (NASA) [74]
148.5-151.5	-159 (N), -189 (L)	705 Aqua (NASA) [75]
155.5-158.5	-163 (N,C)	817 MetOp (EUMETSAT) [76]
164-167	-163 (N,C), -189 (L)	407 GPM Core Observatory (NASA/JAXA) [33]
174.8-191.8	-163 (N,C), -189 (L)	407 GPM Core Observatory (NASA/JAXA) [33]
226-231.5	-160 (N,C), -194 (L)	705 Aura (NASA) [74]
235-238	-194 (L)	705 Aura (NASA) [74]

Table V: Passive sensing satellites in different bands above 100 GHz, with the maximum interference level set in [23]. N stands for Nadir scan, C for conic, L for limb.

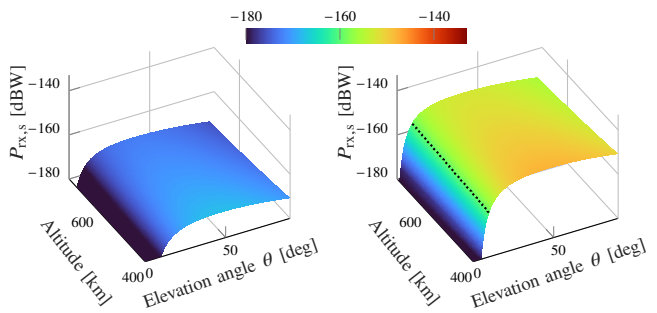
reported for transmit power and effective isotropic radiated power in current sub-6 GHz and lower mmWave backhaul deployments [72], [73].

Table V lists the satellite which, for a given frequency band, occupies the lowest altitude orbit. The maximum permissible interference level is defined in [23]. The RFI level changes according to whether the scan is performed in Nadir, Conic, or Limb mode, i.e., according to the orientation and angle between the ground RFI emitter and the antenna of the satellite under consideration. With a Nadir scan, the satellite sensor and/or antenna points to the ground directly below the satellite (i.e., the Nadir direction). With a Limb scan, the sensor and/or antenna points to the edge of the Earth as seen by the satellite. With a Conic scan, the satellite can sense in different directions (cones, or beams) over time. The RFI threshold is also defined independently on the specific scientific mission and the altitude at which satellites orbit. Therefore, we consider this as a reference for harmful RFI in the next paragraphs.

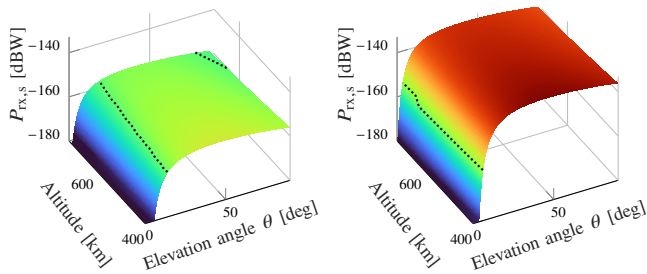
Figure 10 analyzes the RFI for satellites performing a scan at $f_c = 230$ GHz. We assume Nadir/Conic operations, for which the corresponding RFI threshold is -160 dBW. Herein, the ground station antenna has a tilt $\theta_g = 0$ degrees. Additionally, the satellite altitude r ranges from 407 to 720 km, and we consider the two power levels identified in Figure 9b, two different (and constant) gain G_{sat} values for the satellite antenna (i.e., 20 dB and 40 dB), and an elevation angle θ between the satellite and the ground station that varies between 0 and 90 degrees.

With the lowest transmit power and satellite antenna gain (i.e., 18.6 dBW and 20 dBi, respectively), the interference never exceeds the harmful RFI threshold, as shown in Figure 10a. However, when the gain of the satellite antenna increases to 40 dBi, as shown in Figs. 10b and 10d, the interference threshold is exceeded when the satellite orbits above a certain threshold elevation angle, θ_{th} (represented by the dotted line). The value of θ_{th} increases with the satellite altitude. For $P_{tx,g} = 18.6$ dBW (Figure 10b), it ranges from 9.73 degrees at 400 km to 12.26 degrees at 720 km. For $P_{tx,g} = 33.4$ dBW (Figure 10d), it varies from 6 degrees for 400 km to 6.64 degrees for 720 km.

Finally, for $P_{tx,g} = 33.4$ dBW and $G_{sat} = 20$ dBi (Fig-



(a) $P_{\text{tx,g}} = 18.6 \text{ dBW}$, $G_{\text{sat}} = 20 \text{ dBi}$ (b) $P_{\text{tx,g}} = 18.6 \text{ dBW}$, $G_{\text{sat}} = 40 \text{ dBi}$



(c) $P_{\text{tx,g}} = 33.4 \text{ dBW}$, $G_{\text{sat}} = 20 \text{ dBi}$ (d) $P_{\text{tx,g}} = 33.4 \text{ dBW}$, $G_{\text{sat}} = 40 \text{ dBi}$

Figure 10: RFI power $P_{\text{rx,s}}$ at a satellite, as a function of satellite altitude and elevation angle with respect to the ground station, for different values of $P_{\text{tx,g}}$ and G_{sat} . The dotted line represents the combinations of altitude and elevation angle values that lead to $P_{\text{rx,s}} > -160 \text{ dBW}$ (see Table V). $f_c = 230 \text{ GHz}$, $\theta_g = 0 \text{ degrees}$.

ure 10c), satellites at lower altitudes (i.e., below 645 km) experience harmful RFI above the ITU-defined threshold for angles above 13.89 degrees (for 400 km) and 19.3 degrees (for 645 km). The trend is different for higher-altitude satellites, for which there also exists a region at high elevation angles in which the interference is below -160 dBW . Namely, satellites orbiting above 645 km experience RFI above threshold in for elevation angles θ between 19.3 and 89 degrees (for $r = 645 \text{ km}$) and between 21.74 and 81.54 degrees (for $r = 720 \text{ km}$).

To better understand the elevation-dependent RFI trend, we present, in Figure 11, the ground station antenna gain G_g (dotted, left axis), the path gain $-L$ (dashed, right axis), and the overall received RFI $P_{\text{rx,s}}$ for $f_c = 230 \text{ GHz}$, $P_{\text{tx,g}} = 33.4 \text{ dBW}$, and $G_{\text{sat}} = 20 \text{ dBi}$, and $r = 700 \text{ km}$. It is worth noting that for the same satellite altitude r , the distance between the

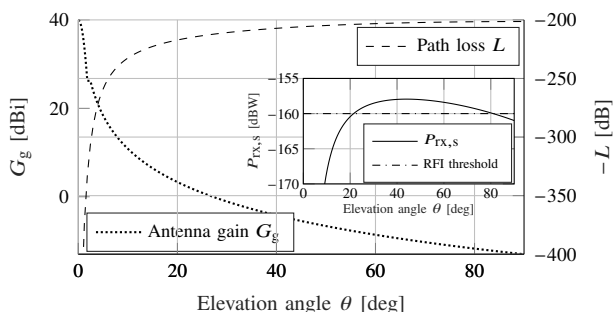
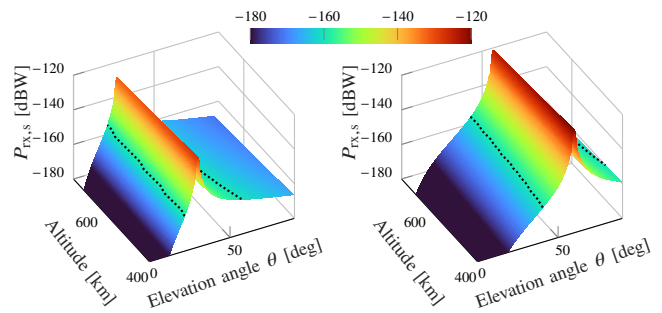


Figure 11: Antenna gain G_g , path gain $-L$, and received power $P_{\text{rx,s}}$ for different elevation angles, satellite height $r = 700 \text{ km}$, $f_c = 230 \text{ GHz}$, $G_{\text{sat}} = 20 \text{ dBi}$, $P_{\text{tx,g}} = 33.4 \text{ dBW}$.



(a) $\theta_g = 30 \text{ degrees}$.

(b) $\theta_g = 60 \text{ degrees}$.

Figure 12: RFI power $P_{\text{rx,s}}$ at a satellite, as a function of satellite altitude and elevation angle with respect to the ground station, for different values of the ground antenna tilt. The dotted line represents the combinations of altitude and elevation angle values that lead to $P_{\text{rx,s}} > -160 \text{ dBW}$ (see Table V). $f_c = 230 \text{ GHz}$, $P_{\text{tx,g}} = 18.6 \text{ dBW}$, $G_{\text{sat}} = 20 \text{ dBW}$.

satellite and a particular ground station is greater for lower elevation angles, i.e., when the satellite is closer to the horizon. Additionally, the signal has to travel through a thicker portion of the Earth's atmosphere, further increasing the contribution of the absorption loss. Therefore, even if the antenna gain of the ground station antenna is maximum at $\theta = \theta_g = 0 \text{ degrees}$, the high path loss leads to a RFI below the defined threshold. The path loss, however, decreases faster than the gain as a function of the elevation angle θ , as shown in Figure 11. This leads to an increase in $P_{\text{rx,s}}$, which—in this specific case—exceeds the ITU threshold for $\theta > 21 \text{ degrees}$. Finally, the path loss flattens for elevation angles above 50 degrees, while the antenna gain decreases logarithmically with θ . Therefore, there can be combinations of path loss, transmit power, and antenna gain values that lead to RFI being below the ITU threshold for high elevation angles (i.e., for the satellite orbiting above the ground station).

We also consider the case in which the ground station antenna points toward the sky with a positive tilt θ_g . This is a typical representative of 6G non-terrestrial use cases, such as satellite-assisted cellular networks [77], the space Internet [78], and drones and UAV aerial networks [79], [80]. Figure 12 reports the received power at the satellite for $P_{\text{tx,g}} = 18.6 \text{ dBW}$ and $G_{\text{sat}} = 20 \text{ dBi}$, and the antenna on the ground tilted by $\theta_g = 30 \text{ degrees}$ and $\theta_g = 60 \text{ degrees}$. Notice that with $\theta_g = 0$, the RFI for this configuration of transmit power and satellite gain does not exceed -160 dBW (Figure 10a). Our analysis shows that there exists a tilt angle $\theta_{g,\text{th}} = 7.2$ for which combinations of $\theta_g \geq \theta_{g,\text{th}}$, θ , and r lead to RFI above threshold. In particular, the satellite receives RFI as high as -127 dBW for $\theta_g = 30 \text{ degrees}$ (Figure 12a), and -119 dBW for $\theta_g = 60 \text{ degrees}$ (Figure 12b).

These analyses indicate that directional antennas can come with mixed blessings: while the combination of directivity and high atmospheric absorption helps reducing RFI in some scenarios (low satellite elevation), the same can lead to extremely high RFI for higher satellite elevation and non-terrestrial communications scenarios. Finally, while we consider ground-to-satellite RFI herein, similar insights can be derived when investigating interference from aerial sources toward ground

passive scientific infrastructure, e.g., for radio astronomy. Indeed, while terrestrial radio astronomy sites are generally isolated and in remote locations, sidelobes (or, more rarely, main lobes) from aerial sources have the potential to generate harmful interference to passive terrestrial stations, as discussed in Section III.⁶

V. SPECTRUM SHARING TECHNIQUES ABOVE 100 GHz — CHALLENGES AND OPPORTUNITIES

The results of Section IV highlight that there exist scenarios in which active transmissions can create interference toward passive users, despite the directional nature of the signals and the high absorption and spread loss. At the same time, however, they suggest that in-band sharing in the spectrum above 100 GHz may be possible, thanks to the combination of the molecular and spreading path losses and the directional transmissions. Therefore, to enable dynamic spectrum sharing solutions, it becomes necessary to identify some technological enablers that allow network operations in a regime where (i) interference is reduced or eliminated, or (ii) shared usage is enabled on a spatial, time, or frequency/band basis. The next paragraphs discuss the technological challenges to spectrum sharing above 100 GHz, with prospective solutions that span from devices and RF circuits engineering (antenna solutions, innovative intelligent surfaces) to the design of communication and sensing stacks. Note that some of these technologies are in use—or can be used—also in other frequency bands, but they often require adaptations or addressing specific engineering challenges to be effective or feasible above 100 GHz, as we discuss in the *Research challenges* paragraphs of this section.

A. Challenges to Spectrum Sharing Solutions Between Active and Passive Users Above 100 GHz

Spectrum sharing has been widely studied in the sub-6 GHz domain, as mentioned in Section I [10], [84]–[86]. A significant effort has been put into identifying spectrum sharing solutions for example in the context of Radio Access Network (RAN) sharing among multiple 5G operators [84]. So far, however, most of the research has focused on sharing among active users and, in particular, between communications users. As mentioned above, several of the techniques investigated for the bands below 6 GHz and active users sharing do not necessarily apply to sharing among active and passive users above 100 GHz, or require solving significant engineering challenges.

For example, one of the main areas of research is cognitive radios [85]. In this approach, dynamic spectrum access of secondary users over resources primarily destined for other users is enabled with a two-step approach. The first step involves sensing or collecting information on spectrum usage, thereby identifying unused portions of the spectrum and/or

patterns of usage of the primary users. The second step involves secondary-user transmission. This can happen on unused resources (interweave mode) or on the resources already occupied by the primary (overlay mode), possibly with some coordination to satisfy predefined interference constraints. Notably, cognitive radios have been popular in the context of improving the usage of TV white space [87]. However, the paradigm of cognitive radio cannot be applied directly to active-passive sharing above 100 GHz. The “sensing” step is challenged by several conditions. The spectrum access by passive users cannot be sensed. The increased directivity and large bandwidth requirements of active-user transmissions make detection more complex. Along these lines, the scale (in the number of devices) envisioned for certain above-100-GHz applications [16]⁷ further complicates cognitive radio systems, as the overhead for coordination increases and the amount of unused resources for interweave operations decreases. Furthermore, concurrent cognitive transmissions (e.g., as overlay) may not be tolerated by some passive sensing users if further precautions are not applied to avoid exceeding harmful RFI thresholds, as discussed in Section IV.

Other techniques that are broadly considered enablers of spectrum sharing at lower frequencies and for active users cannot be directly applied in the context of active-passive sharing above 100 GHz. Non-Orthogonal Multiple Access (NOMA) [89], which enables code-based or power-based sharing of the same time and frequency resources among multiple users, has been designed for the coexistence of multiple active users. Similarly, sharing across licensed and unlicensed bands does not apply when passive users are at stake [90]. While [91] and [92] consider coexistence between communication users and passive RAS and EESS services, these are for frequency bands below 100 GHz.

An additional challenge is represented by the heterogeneity between the different technologies at these frequencies [10], which require either custom solutions or coordination among different standardization or technology development forums. Such coordination, however, has been shown to be previously feasible in the sub-6 GHz context, with the notable example of the CBRS band. This portion of the spectrum, which was exclusively allocated to military use (e.g., US Navy radars and satellite links), is now operated according to a shared usage pattern, facilitated by an inter-technology database that keeps track of spectrum usage and grants access with high granularity.

Overall, it is clear that there exists a need to carefully design and re-think enabling technologies and strategies to allow sharing between active and passive users in the 100 GHz bands. In addition to accounting for the presence of passive users, spectrum sharing above 100 GHz should also factor in and exploit the unique characteristics of the propagation of RF signals in these bands [93]. To this end, in the next paragraphs, we discuss and review techniques that can be applied for effective and safe active/passive sharing at frequencies above 100 GHz.

⁶Notice that large satellite constellations also have the potential to affect ground based *optical* telescopes used for astronomy and planetary defense, i.e., to track satellites and near-Earth asteroids. However, it has been found that the impact from Low Earth Orbit satellites is quite manageable, as their reflected sunlight is rarely bright enough to cause major problems, except when they are very close to the horizon where these telescopes rarely operate [81].

⁷Projections from literature and market analysis point to an increase from 10^6 to 10^7 devices per km^2 when transitioning from 5G to 6G [88].

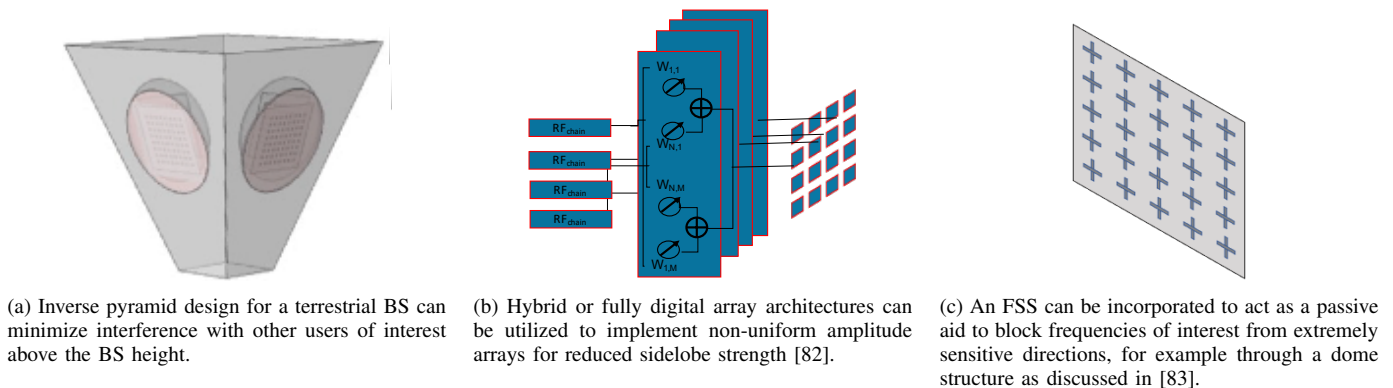
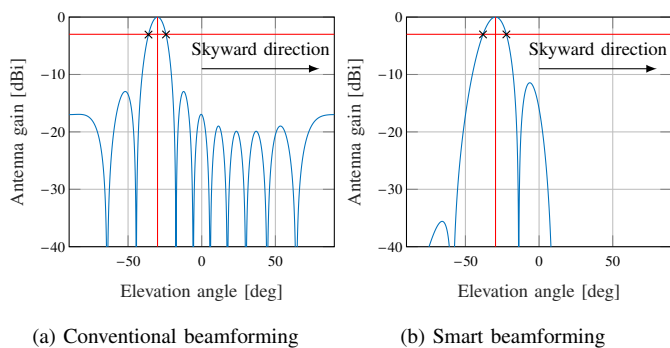


Figure 13: Device configurations to minimize undesired RFI.

Figure 14: The utilization of active suppression on the skyward directions during the array synthesis can suppress unwanted emissions. In both cases, the desired angle of steering is 30° below the horizon.

B. Solutions enabled by (sub) Terahertz Devices and Wave Propagation

To effectively communicate at frequencies above 100 GHz, highly efficient, directional antennas are required. In such a setup, unwanted interference toward sensitive devices outside the main coverage region manifests as leaking power in the form of side-lobes. In directional antennas as well as uniform amplitude antenna arrays, the more directional the mainlobe, the greater the dominant side-lobe-levels (SLL), or the effective power contained within the dominant sidelobes [82]. Such a manifestation of the sidelobes can be seen for a typical high density MIMO array (8×8) in Figure 14a. It is seen that, while the mainlobe can be extremely directional, the major sidelobe strength can be as much as -13 dB in comparison. Thus, it is necessary to consider the entire radiation pattern of the array/antenna, and develop working objectives to truncate such SLL which contribute to interference concerns.

Inverse Pyramidal Arrays. Above 100 GHz, highly directive radiation as well as significant power output is expected for base stations (BSs) supporting massive MIMO. Thus, the main objective of device design can be tailored towards significant control over the SLL in these BSs. An intuitive method of mitigating interference in unwanted directions is to have a physical configuration within which the unwanted directions are generally excluded from the radiation pattern. The inverse pyramidal array design, an example of which is presented in Figure 13a, acts as a direct complement to the

pyramidal array design [94]. In such a setup, the geometrical configuration of the array favors scan angles below the horizon, thereby minimizing the power leakage above the BS itself. A four-sided pyramidal array, similar to that in Figure 13a, is known to provide maximum coverage efficiency, thereby reducing deployment resources [94]. Each side of the pyramid comprises an antenna array that serves a particular sector, for full coverage.

Research challenges: It is important to note that this design can be used only in deployments with BSs altitude higher than that of the connected users. In addition, there are multiple research challenges related to building dynamic beamforming antenna arrays above 100 GHz, as we describe together with the next point.

Active SLL Suppression. As mentioned in Section IV, 6G BSs may be required to provide coverage in aerial scenarios. Here, the BS needs to serve users not just at lower or at equivalent altitudes to itself (e.g., other BSs and User Equipments (UEs)), but also to users above in altitude, for example, UAVs. Thus, in the full 3D coverage space, it becomes necessary to consider more active SLL suppression techniques. In conventional arrays, zero-forcing beamforming is considered a convenient technique, with which different receivers can experience orthogonal channels. In this case, the goal of the beamforming algorithm is to ensure that no signal is received in a target direction, at the cost of less control on the beam shape everywhere else. However, with fully digital or even hybrid beamforming architectures as found in current massive MIMO 5G devices [95], more robust beamforming techniques can be implemented. We present an example of a hybrid beamforming architecture that could be exploited to control interference in Figure 13b, with the corresponding potential far-field radiation response shown in Figure 14b. With knowledge of critical interference directions (where sensitive devices may be located) the array response can be tailored through interference suppression algorithms as in [96], to ensure complete suppression of leakage in critical directions, while still providing coverage to users that require service in other angular regions. As shown in Figure 14b, the mainlobe can be preserved while the more problematic sidelobes can be truncated greatly.

In addition to novel array architectures, another breakthrough that is extremely important in the above 100 GHz

range is the rise of intelligent reflecting surfaces (IRSs) [97]. Although the fundamental principles of IRSs are valid across the spectrum, these are increasingly relevant for the (sub-)THz band, as the greatly simplified design helps to reduce the constraints on increasing the size of the array and in its deployment [98]. For example, the reflectarray-based IRS demonstrated in [98] is composed of nearly 10,000 elements, while active RF chain-based arrays are yet below the 256-element mark [99]. By moving the burden of beamforming “off-chip”, and removing the need for any RF chains, the same IRS can be shared among multiple users, as discussed [100]. IRSs can also be manipulated to create custom beam shapes [100], and if their design is realized through a metasurface-based, sub-wavelength-sized meta-atoms, the level of control is increased drastically [97], [101]. Such IRSs can be utilized to create anomalous reflection [102], in which almost negligible sidelobes are produced, greatly reducing interference due to sidelobe energy and introducing new opportunities for spectrum sharing. They can also be used to redirect beams towards different directions from where originally intended, as discussed in [103].

Research challenges: The majority of algorithms for beam design and active SLL suppression have been proposed for lower-frequency systems and, thus, do not capture challenges associated with working above 100 GHz. As we move to higher frequencies, the wavelength becomes shorter and, thus, the antenna array elements become smaller and they can be more densely packed without suffering mutual coupling [50]. However, the size of every other component in the RF chain (i.e., frequency multipliers, mixers, filters, and amplifiers) does not necessarily scale by the same factor. This leads to challenges in packaging of such arrays above 100 GHz. Consequently, there is a need to develop new antenna array architectures. First, one could consider adopting a fully analog antenna architecture, in which one only RF chain is utilized to drive multiple antennas each with analog phase and/or amplitude control [104]. Even in that case, there are several challenges. First, broadband phase controllers that can work across large contiguous bandwidths (e.g., tens of GHz) are still being developed. Strictly speaking, some of the benefits shown in Figure 14b could be achieved only with the additional manipulation of the amplitude at each antenna element [82], [105]. However, the integration of an amplitude controller (ultimately, a power amplifier) per antenna element is many times not possible again not only due to packaging but also thermal issues [99]. As a solution, innovative true-time delay controllers could be utilized, for example by leveraging new materials such as graphene specifically proposed for the terahertz band [106] and, accordingly, the algorithms adapted.

Many of the challenges associated with building such antenna arrays and IRSs originate in the fact that the designs demonstrated to date leverage the so-called electronic approach to sub-THz and THz devices [27], in which the limits of traditional electronic systems are pushed to operate at higher frequencies. Alternatively, again new materials could be adopted to build arrays that leverage the properties of surface plasmon polariton waves and intrinsically operate at

THz frequencies [50]. As of today, graphene-based plasmonic signal sources [107], [108], plasmonic phase, amplitude and frequency modulators [109], [110], and antennas [111] have been demonstrated. Their integration in very dense arrays with element spacing much smaller than the free-space wavelength enables ultra-massive MIMO systems [112], with unprecedented control of the beam shapes and wavefronts [100]. Nevertheless, this technology is much less mature than electronic or even photonic solutions, making it a high-risk, high-reward approach. Even with IRSs, although it is much easier to scale up in size, designing high-performing, versatile analog phase shifters at such high frequencies is a challenging task [113]. Among other solutions, the utilization of plasmonic materials and hybrid structures presents an interesting direction for realizing these devices [114].

Passive Mitigation Techniques. In addition to preemptive suppression techniques at the BS, it is possible to address interference through passive devices that do not increase the complexity of the BS itself. From the discussions in Section II-A and IV, it is evident that sensitive devices which require protection from unwanted interference will rarely occupy the entire spectrum of emission of the BS. For example, the presently prohibited 109.5 GHz to 111.8 GHz portion of the spectrum can be specifically addressed by suppressing RFI within this 2.3 GHz bandwidth. In this regard, Frequency Selective Surfaces (FSSs) are devices that specifically address such sensitive specks of a frequency spectrum. As shown in Figure 13c, an FSS is a dense, metasurface-like configuration with resonant passive elements in an array, usually designed to intercept and interact with a bandwidth of interest [115]–[117]. These have traditionally been utilized to reduce the cross-section of radars [115], and recently have been proposed to reduce unwanted SLLs and leakage in wide-band antenna arrays above 100 GHz [118]. In addition, these have been proposed to reduce mutual coupling effects between antenna elements in densely packed antenna arrays [119]. Within the mmWave band, FSSs have attracted attention, inter alia, to act as planar lenses with enhanced directivity, low cost, and ease of deployment [116], [117]. With an FSS, it is possible to design both band-stop and band-pass filters that can be deployed without any additional complexity at the BS itself, avoiding the complexity of greater control and increased power consumption requirements. The effectiveness of an FSS depends on the relative orientation of the surface with the unwanted radiation. Thus, with proper alignment towards the dominant sidelobes that may interfere with sensitive devices, an FSS designed to act as a stop-band at the sensitive portions of the spectrum can be deployed, through which the unwanted leakage can be suppressed significantly [115].

Research challenges: While simpler than the devices needed for active SLL suppression, the main challenges associated with the passive solutions relate again to the hardware design. In particular, when implemented through metasurfaces, the design of the FSSs is not governed by well-defined equations and operating theory as, for example, the design of beamforming or beam-nulling algorithms. Instead, an “artisan” based trial-and-error methodology is required to develop the meta-atom shape and arrangement [101], [120]. As an alternative,

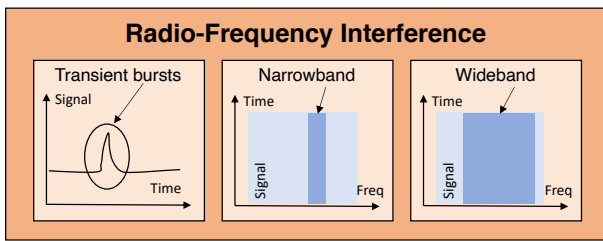


Figure 15: Classification of different sources of RFI.

a library of meta-atoms designs and potential arrangements to achieve different functionalities needs to be built, which could benefit the wireless community at large. In addition, there are system level challenges associated to deploying such devices, in terms of both network and frequency planning.

C. Solutions based on RFI Mitigation for Passive Users

Complementary and independent of custom device design solutions, harmful RFI can be mitigated with signal processing techniques. RFI mitigation has been typically studied as a necessary step in passive sensing signal processing pipelines, to protect from undesired RF emissions in the band of interest, either intentional or unintentional. As discussed in Section II, the receivers used by several passive sensing applications (e.g., radio astronomy) have extremely high sensitivity and can pick up signals that would otherwise be considered below the noise floor [121]. In the context of spectrum sharing, RFI mitigation puts the burden of the interference management on the passive users. Therefore, while it is an essential component of the passive sensing digital signal pipeline, it represents just one of the different ingredients that need to be combined for a balanced approach to spectrum sharing. In the next paragraphs, we review general characteristics and approaches for RFI mitigation, and discuss a few specific examples of RFI mitigation above 100 GHz.

RFI is generally categorized in three different classes (Figure 15), i.e., transient bursts, generated by impulse-like waveforms, and narrow-band or wide-band signals. Additionally, RFI may be caused by sources that transmit in the band of interest, or by out-of-band emissions. The RFI may (i) introduce clearly identifiable distortion(s) in the gain or frequency response of the received waveform; (ii) obscure the received signal, with a strong and identifiable emission in the entire observed spectrum; or (iii) introduce more subtle alterations in the received signals (e.g., if the RFI power is close to the noise threshold), which are harder to detect and, consequently, filtered out.

General RFI Mitigation Techniques. The general approaches toward RFI mitigation involve temporal, frequency, or spatial filtering, or rely on specific properties of the received signals. Temporal and frequency domain RFI can be detected and blocked if confined in specific time instants or sub-bands, for example with threshold-based methods. For measurements of natural phenomena, whose statistical distribution is known (and often Gaussian), statistical methods can be used to identify and reject outliers that may correspond to RFI [122]. Widely used techniques include (i) evaluating the kurtosis ratio

of the received signal [123], i.e., the ratio between the fourth moment and the squared second moment (variance) of a signal, which should be equal to 3 for Gaussian signals; and (ii) evaluating the third and fourth Stokes parameters of the signal, which are related to its polarization and are typically small in the absence of RFI [122]. The RFI can also be detected by analyzing signals in the spatial domain. If the direction of the source of the intended signal is known, RFI can be detected through filtering signals with Angle of Arrival (AoA) outside a pre-defined region [121]. Importantly, as discussed above, the presence of massive-MIMO arrays in the 100 GHz region provide an ability of unprecedented angular resolution and accurate AoA detection. Alternatively, highly diffused sources without RFI exhibit a smooth behavior in the spatial and angular domain, thus RFI can be detected and filtered by analyzing the outliers. State-of-the-art RFI mitigation systems often combine two or more of these techniques, to maximize the probability of detecting RFI [124]–[126].

Use-case-specific RFI Mitigation Techniques. The RFI mitigation techniques need to adapt both to the characteristics of the interferer and to the nature of the observation and equipment utilized. The result is that, oftentimes, general signal processing techniques for RFI mitigation need to be adapted to the specific use case [121], [126]–[128]. Signal processing for RFI mitigation can be run offline [129] or online [130]. While this may be a concern for the spectrum above 100 GHz, given the large bandwidth at stake, the research and development of hardware-accelerated signal processing pipelines has led to multi-carrier filter banks capable of processing tens of GHz of bandwidth [131]. Similarly, mixed online and offline approaches are emerging to reap the benefits of both, e.g., for the RFI mitigation system of the next-generation Very Large Array (ngVLA) radio telescope [132]. This enables both real-time adaptability to the source and more complex signal processing offline, with applicability to very large bandwidths. While the ngVLA is expected to work in the 1.2-116 GHz band, the hardware and software techniques developed for its RFI mitigation could be re-used in above-100-GHz systems as well.

Research challenges: So far, most of the research on RFI mitigation has focused on sensing bands below 24 GHz [133], which were considered the most exposed to undesired emissions from commercial radios. This represents a potential issue for current systems operating above 100 GHz, as they are generally not equipped with RFI mitigation pipelines, which reduces the ability for sharing and coexisting with active systems. Future sensing instruments can instead be equipped with RFI mitigation mechanisms, whose design, however, is challenged by a number of elements. As previously mentioned, the large bandwidth complicates the design of real-time signal processing pipelines for RFI mitigation. In addition, the design of RF circuits is made more complex by the high frequency and large bandwidth requirements, which may introduce greater interference from out-of-band emissions. However, the limited multipath (or absence of it) typical of propagation above 100 GHz [134] makes spatial filtering extremely powerful, as RFI sources exhibit limited or no scattering and the number of directions to target for nulls

become smaller.

D. Solutions based on Waveform Engineering and Digital Signal Processing for Active Users

It is further possible to reduce RFI through waveform designs where the communication and sensing signals are made orthogonal to each other, or are otherwise engineered to not register as interfere with each other.

Spread Spectrum Techniques. A very large contiguous bandwidth can be leveraged to create spread spectrum waveforms, in which the communication signal can be artificially lowered to below the noise floor. Such methods have been utilized in Direct Sequence Spread Spectrum (DSSS) to create efficient spectrum sharing, such as in Code Division Multiple Access (CDMA), where a specific communication signal is multiplied by a spreading key, to artificially spread a narrowband signal over a very large bandwidth [135]. The receiver utilizes the same key to recover the signal, and all other signals within the same sub-space are filtered as noise. In this setup, the larger the pseudo-random key generating sequence, the greater the number of orthogonal signal sets that can be created. In addition, by combining multiple communication bands together, frequency hopping, similar to as in Bluetooth transmission, can be leveraged to create multiple windows of signal transmission that fall outside the critical bandwidth portions reserved for sensing. Ultimately however, such spreading techniques compromise the very high data rate requirement for communication standards, and would require a bandwidth which proportionally increases with the length of the sequence, as compared to that presented in Figure 4b.

Research challenges: As of today, the main bottleneck in DSSS-based coexistence techniques above 100 GHz is the real-time generation of ultra-broadband spreading sequences. For example, in [136], we built and experimentally demonstrated a DSSS system for sharing between active and passive systems above 100 GHz. The framework can successfully generate sequences at 130 GHz with a 20 GHz spread bandwidth. Figure 16 shows the PSD over frequency for a narrowband signal and DSSS signals with three different spreading factors, all for a 4-QAM signal. An increase of the spreading factor leads to more uniform upper envelopes for the PSD, with peaks at about 15 dB below the peak of the narrowband signal, at the cost of achievable data rate. This effect, which is popular in tactical communications contexts to decrease the signal interception or eavesdropping probability, can also lead to received signals at the satellite sensor which are below the RFI threshold, as further discussed in [136]. Indeed, a reduction of 15 dB in the received signal at the passive system can increase the parameter space in which active systems can coexist without exceeding the RFI threshold, e.g., when compared to the configurations in Figure 10. However, to realize this, we used a state-of-the-art arbitrary-waveform generator with data-converters operating at 92 Gigasamples-per-second at the transmitter and 160 Gigasamples-per-second at the receiver, with power requirements, size and cost only suitable for lab testing. To overcome the bottleneck introduced by the high-speed data-converters, one solution is to design

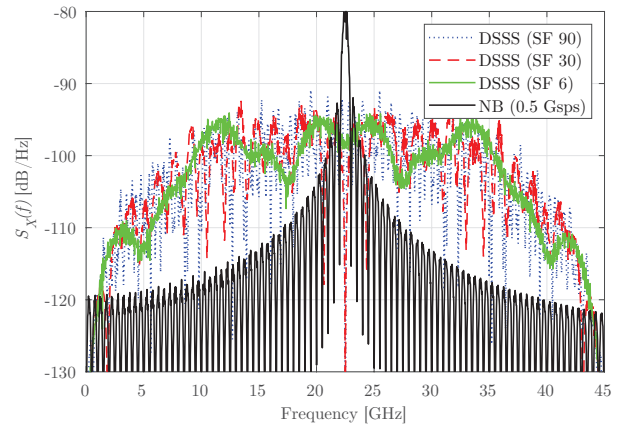


Figure 16: Power spectral density of a DSSS signal with different SF and a narrowband signal, both modulated with 4-QAM. Figure adapted from [136].

fully analog DSSS chips that operate directly with analog I/Q samples in baseband or at an IF frequency. The design of such chips should be accompanied by the exploration of low-complexity real-time implementable orthogonal sequence generation algorithms.

Frequency-Selective Waveforms. Transmitters which can support very high Peak-to-Average Power Ratio (PAPR) can be utilized to actively remove compromised portions of the signal space from waveforms. An example where such a setup could potentially be implemented without significantly reducing the communication capacity is in OFDM [46]–[48]. In OFDM, groups of subcarriers are organized into resource blocks, and power allocation can be performed on a resource block level. The judicious allocation of resource blocks determines the peak capacity rate. In such a setup, it may then be possible to purposely identify sub-carriers within the sensitive regions and minimize the effective power distributed to them.

Research challenges: In alignment with many of the previous challenges, the bottleneck is posed again by the hardware and, particularly in this case, the power amplifiers. At all frequencies but particularly at frequencies above 100 GHz, power amplifiers are very sensitive to power fluctuations and, thus, carrier nulling in OFDM is many times not an option. Besides, waiting on the development of more robust amplifiers, there are other possible solutions. For example, a common waveform found in radar systems, also those at frequencies above 100 GHz, relies on continuous frequency modulation or chirp signals. Recently, our group has demonstrated the ability to utilize chirps in Chirp Spread Spectrum (CSS) to both transmit information even in extreme frequency-selective channels (such as those over an absorption line at THz frequencies) [137] and to build a joint communication and atmospheric radar system [138]. Differently, one could design non-continuous frequency chirps that skip certain frequency bands to minimize the radiation in forbidden bands.

Orthogonal Waveforms. Another technique, only valid for the coexistence of active sensing (e.g., radar) and communication users, relies on utilizing waveforms generated in the context of orthogonal basis sets, where every signal is independent and orthogonal to the other. One such example is

the Gram-Schmidt orthogonalization [139]. In this setup, a set of M finite energy symbols is mapped to a set of N orthogonal symbols as shown in Eq. (16):

$$s_i(t), i = 1, 2, \dots, M \mapsto \phi_i(t), i = 1, 2, \dots, N; N \leq M. \quad (16)$$

Here, the orthogonal signals $\phi_i(t)$ are created from $s_i(t)$ through a filter bank, where the components of the previous orthonormal signals are removed from the concerned signal. Gram Schmidt orthogonalization is actively used in most MIMO applications involving coherent detection by utilizing QR decomposition [140]. Without loss of generality, assume that the first orthogonal signal, $\phi_1(t)$, is actively selected for sensing applications. It is then possible to eliminate any interfering portions from the remaining symbols, $\{\phi_2(t), \phi_N(t)\}$, used for communications. This procedure requires some level of interaction between the active sensing and communications systems to coordinate on the nature of the sensing signal $\phi_1(t)$.

It is important to note that the exclusion of an orthonormal basis function does not simply remove one symbol from the possible symbol set of transmission. In fact, this makes the symbol set incomplete, reducing it from $M = 2^N$ to $M - 1 = 2^N - 1$, thus making the representation of N bits impossible. Thus, with the capability of representing only $N - 1$ bits, only $2^{(N-1)} = M/2$ symbols are required.

Here, we observe that this setup can still be utilized when required to preserve multiple sensing frequencies since there are several redundant message symbols that can be utilized and thus could be utilized without losing any further capability. Ultimately however, the principles of utilizing the Gram Schmidt orthonormalization require careful consideration of the richness of the basis set, the complexity of the modulation scheme, and the modifications that must be performed with regard to ensuring the key system parameter such as the bit error rate, the data rate, and the Euclidian separation of the constellation points can be determined accurately and predictably.

Research challenges: This type of solution is only applicable to future active and passive coexisting systems, as it requires coordination. As mentioned in Section III-C, this is the type of “burden sharing” expected from Resolution 731. As with the other waveforms-based solutions, the computational complexity of the modulation/demodulation algorithms, the requirements on the data-converters, and the potential implementation of the solution in the analog domain are aspects to be taken into account. In addition, the modulations utilized in high data rate communications often require precise inputs and constellation requirements, which makes the omission of a basis function particularly challenging. Certain parameters such as a uniform constellation, the efficiency of a message signal, and a possible non-completeness of the symbol set could result in non-linear distortions as well as reduced throughput, as discussed above.

E. MAC Layer and Networking-based Sharing

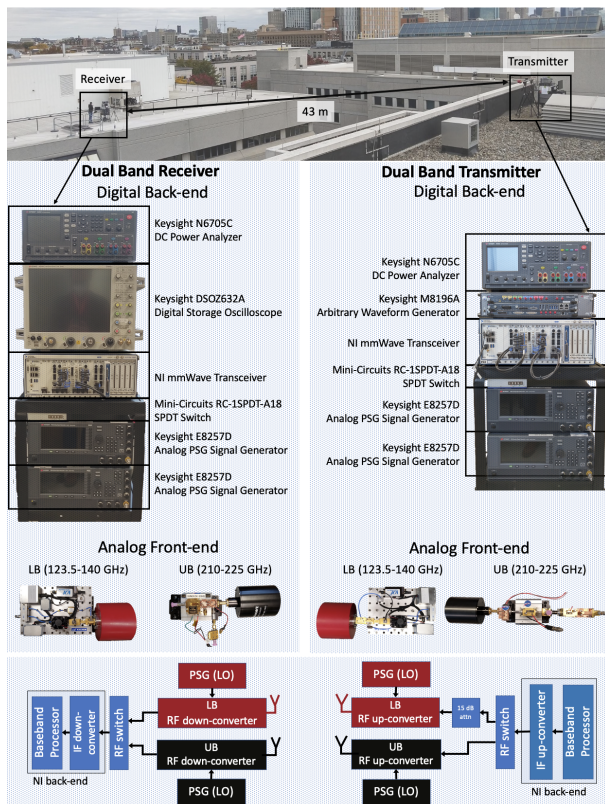
Dynamic spectrum access can be enabled at the MAC layer and above through time and spatial sharing. In particular, it is possible to envision sharing mechanisms with different levels

of integration among the technologies used by interested stakeholders of the above 100 GHz band, from a fully integrated solution to a CBRS-like model.

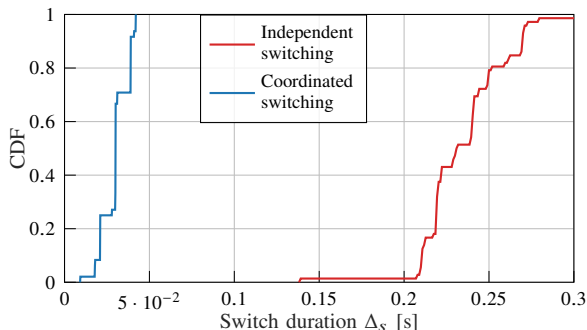
Shared Active / Passive Medium Access Schemes. One option is represented by Time Division Multiple Access (TDMA) between two or more technologies, with active and passive users sharing different time resources. For example, next-generation wireless network MAC designs may include some time slots that can be blanked for sensing [141], either active or passive. To fully exploit this flexibility, the sensing stack could be integrated in the communications stack, e.g., satellites used for commercial downlink communications could be also equipped with passive sensing systems activated on a time-sharing basis. Alternatively, passive sensing systems could be equipped with an additional sensing loop that detects when the communication link is not used and collect valid observations.

Research challenges: It is challenging to design, deploy, and implement these approaches in practice. Indeed, they require a tight synchronization between different signal processing chains and RF circuits, which generally have a transient behavior and cannot switch on and off instantaneously [143]. Therefore, even though this is a MAC-level strategy, it requires tight coordination and innovations in physical layer and at the device level, especially as the duration of channel access decreases with the increase of the data rate. Additionally, while frequent time-switching is well tolerated by packet-based communications systems [144], [145], it may not be compatible with the sensing of continuous sources of electromagnetic signals and/or long integration times. Finally, these sharing solutions are dependent on protocols that would need to be developed, tested, and standardized in the relevant forums.

Multi-band Systems. It is also possible to design time sharing mechanisms with a granularity in the order of minutes. While these do not enable the same level of multiplexing and spectrum utilization as MAC-based strategies, they require limited or no coordination between the users of the spectrum. Notably, there are approaches in which only one of the two systems (i.e., communications or sensing) can change to adapt to the other. For example, in [142] we demonstrated the feasibility of passive/active spectrum sharing through dynamic spectrum access, with the communications stack dynamically adapting to the presence of passive sensing satellites over the deployment area. The system (shown in Figure 17a) is capable of tracking satellite mobility (e.g., the NASA Aura satellite [4]) and predict when a passive-sensing station starts orbiting over the deployment area of the communication link. When this happens, the systems switches from the band that may interfere with the satellite to another band, enabling time-sharing of resources that would otherwise be unused, while introducing no harmful interference to the sensing system. This process happens with a granularity of minutes, i.e., it does not need a tight integration between the sensing and communications stacks. Nonetheless, it is important to perform the switch between bands in a timely fashion, so as to avoid downtime for the communication link. Figure 17b compares the CDFs of the duration of switch events with a coordinated (or centralized) approach and an independent



(a) Prototype schematics of a dual-band prototype for dynamic spectrum access above 100 GHz, from [142].



(b) Cumulative Distribution Function (CDF) of the duration of a procedure to switch between bands, with a centralized (coordinated) or distributed (independent) approach, from [142].

Figure 17: Prototype and performance of the first dynamic spectrum access system above 100 GHz, from [142].

(or distributed) strategy. Even though this is a prototype, the system achieves low switching times (i.e., in the order of ms) with the centralized switching, showing that dynamic spectrum access is feasible even in the spectrum above 100 GHz.

Research challenges: There are several system-level challenges that need to be addressed to make these schemes scalable and practical. As for the MAC-based approaches, there is a need for protocols and standardized strategies. In this sense, the transition toward more open and programmable systems in cellular networks [146] will help embedding dynamic control of the cellular stack and provide practical primitives to implement this kind of spectrum sharing. Besides this, other system-level challenges are related to security, scalability, and

resource scheduling, in particular considering the directional nature of communications above 100 GHz and the number of users that will need to be supported in 6G systems.

Coordination-based Sharing. From a broader perspective, dynamic spectrum access can be generically extended to support the coexistence of multiple services, for example through a shared, dynamic spectrum marketplace (which could be managed by the ITU or by local regulators) in which licenses can be leased dynamically, with a sub-second latency. As previously mentioned, the CBRS band proceedings have shown that coordination and preemption among different active users is feasible on a dynamic basis. In [147], [148], the authors demonstrate a dynamic system for active/passive users sharing as part of one of the DARPA Spectrum Collaboration Challenge (SC2). The availability of fast connectivity and data bases is a key step toward the feasibility of distributed spectrum access systems that can control spectrum usage with granularity of tens of kilohertz in bandwidth and 1 ms in time (typical values for 5G systems) [149]. Coordination-based solutions are also mentioned and evaluated in the National Research Council report on how spectrum can be used by scientific users in the 21st century [22]. The authors envision a scenario with multiple satellites for Earth exploration, each with a beam covering an area on Earth with a diameter of 30 km. The active users on the ground could coordinate with the sensing satellites through a shared database and blank the resources required for sensing on an ad hoc basis. For a constellation of 30 satellites, with the aforementioned characteristics, the authors of [22] estimate that active users can transmit in the band of interest of the passive sensing system for 99.7% of the time *without causing any interference*. Similar results are presented in [150]. This shows that spectrum sharing between active and passive users is possible, with the proper combination of policies and technologies.

Research challenges: As for the previous higher-layer techniques, most challenges arise at the system level, in particular when considering the number of active and passive users that require coordination, the size of the database, and the need for real-time adaptation. A promising factor is that there is a limited number of passive sensing facilities, whose position and frequency occupation is often known or predictable, and by the fact that terrestrial sensing stations (e.g., for radio astronomy) are in remote locations with limited human presence. Nonetheless, any solution that has the potential to be deployed in practical scenarios needs to be tested for robustness, scalability, and security, without harming passive users in the process, while guaranteeing the data rates and quality of services levels expected for above-100-GHz communications systems. Finally, sensing- and beaconing-based coordination (e.g., as CBRS) are challenged by the directional nature of communications above 100 GHz, which could introduce deafness to some transmissions or beacons.

VI. CONCLUSION

The future of technologies and policies in the spectrum above 100 GHz is being shaped by the development of new use cases and capabilities in the communications and active

and passive sensing domains. In this paper, we have provided the first comprehensive overview of stakeholders, policies, and technologies for spectrum sharing in the band above 100 GHz. First, we reviewed the relevance of this portion of the spectrum for sensing applications in both the active and passive sensing domains, and for next-generation communication networks. We discussed the need for more bandwidth for improved performance in both sensing and communication applications, which motivates spectrum sharing approaches, and reviewed the relevant spectrum policies in this domain. We then analyzed the impact that active terrestrial users may have on passive sensing satellites, showing how spectrum sharing techniques need to protect and account for the presence of passive incumbents. Finally, we discussed possible approaches to spectrum sharing above 100 GHz, considering devices, signal processing, and higher-level coordination.

Outlook — Spectrum Policies for the Next Decades

The paper clearly shows that there exists need, opportunities, and technologies to enable a shared use of the spectrum above 100 GHz. In this sense, the sensing and communication communities have the opportunity to work together to evolve spectrum policies and technologies. Efforts in this direction can lead to:

- enabling experimental research on spectrum sharing between active and passive users, fully realizing the provisions in the ITU Resolution 731 [26], and jumpstarting the development of technologies for safe spectrum sharing above 100 GHz. In this sense, the development of National Radio Dynamic Zones (NRDZs) will be critical for the study of active/passive coexistence. The U.S. National Science Foundation NRDZ program seeks to establish large-scale testbeds in contexts where RF transmissions outside current regulations will not harm normal receivers. Through this program, we are developing NRDZ capabilities in Colosseum, an open-access and publicly available hardware-in-the-loop wireless network emulator [151]. Colosseum will be extended to support large-bandwidth, highly directional transmissions (such as those of interest in the spectrum above 100 GHz), and is naturally positioned for spectrum sharing studies without any risk of harming legitimate users of the spectrum thanks to its emulation capabilities;
- identifying opportunities for a sharing-aware approach for the development of future scientific sensing equipment and communication networks. For example, active engagement across different communities could lead to the establishment of sharing procedures similar to that of the CBRS band, with benefit for all parties involved;
- using an evidence-driven, physics-based approach to develop spectrum policies that involve sharing in the RR5.340 bands, without harming passive incumbents.

REFERENCES

- [1] I. F. Akyildiz, J. M. Jornet, and C. Han, "Terahertz band: Next frontier for wireless communications," *Physical Communication*, vol. 12, pp. 16–32, September 2014.
- [2] P. U. Jepsen, D. G. Cooke, and M. Koch, "Terahertz spectroscopy and imaging—modern techniques and applications," *Laser & Photonic Reviews*, vol. 5, no. 1, pp. 124–166, January 2011.
- [3] R. Dickie, R. Cahill, V. Fusco, H. S. Gamble, and N. Mitchell, "THz Frequency Selective Surface Filters for Earth Observation Remote Sensing Instruments," *IEEE Transactions on Terahertz Science and Technology*, vol. 1, no. 2, pp. 450–461, Nov 2011.
- [4] J. W. Waters *et al.*, "The Earth observing system microwave limb sounder (EOS MLS) on the aura Satellite," *IEEE Transactions on Geoscience and Remote Sensing*, vol. 44, no. 5, pp. 1075–1092, May 2006.
- [5] G. B. Taylor, C. L. Carilli, and R. A. Perley, "Synthesis imaging in radio astronomy ii," *Synthesis Imaging in Radio Astronomy II*, vol. 180, 1999.
- [6] C. E. Shannon, "A mathematical theory of communication," *The Bell system technical journal*, vol. 27, no. 3, pp. 379–423, July 1948.
- [7] J.-S. Lee and E. Pottier, *Polarimetric radar imaging: from basics to applications*. CRC press, 2017.
- [8] 3GPP, "Study on supporting NR from 52.6 GHz to 71 GHz," TR 38.808, Rel. 17, 2021.
- [9] J. Hasch, E. Topak, R. Schnabel, T. Zwick, R. Weigel, and C. Waldschmidt, "Millimeter-Wave Technology for Automotive Radar Sensors in the 77 GHz Frequency Band," *IEEE Transactions on Microwave Theory and Techniques*, vol. 60, no. 3, pp. 845–860, March 2012.
- [10] A. M. Voicu, L. Simić, and M. Petrova, "Survey of Spectrum Sharing for Inter-Technology Coexistence," *IEEE Communications Surveys and Tutorials*, vol. 21, no. 2, pp. 1112–1144, Second quarter 2019.
- [11] J. M. Jornet and I. F. Akyildiz, "Channel Modeling and Capacity Analysis for Electromagnetic Wireless Nanonetworks in the Terahertz Band," *IEEE Trans. Wireless Commun.*, vol. 10, no. 10, pp. 3211–3221, Oct. 2011.
- [12] D. Mittleman, *Sensing with terahertz radiation*. Springer, 2013, vol. 85.
- [13] M. Caris *et al.*, "Very high resolution radar at 300 GHz," in *2014 11th European Radar Conference*, 2014, pp. 494–496.
- [14] J. Kokkonen, J. Lehtomäki, and M. Juntti, "A discussion on molecular absorption noise in the terahertz band," *Nano Communication Networks*, vol. 8, pp. 35–45, June 2016, electromagnetic Communication in Nano-scale.
- [15] M. Giordani, M. Polese, M. Mezzavilla, S. Rangan, and M. Zorzi, "Toward 6G Networks: Use Cases and Technologies," *IEEE Commun. Mag.*, vol. 58, no. 3, pp. 55–61, March 2020.
- [16] M. Polese, J. M. Jornet, T. Melodia, and M. Zorzi, "Toward End-to-End, Full-Stack 6G Terahertz Networks," *IEEE Communications Magazine*, vol. 58, no. 11, pp. 48–54, November 2020.
- [17] A. F. Shehab, M. A. Elshafey, and T. A. Mahmoud, "Recurrent neural network based prediction to enhance satellite telemetry compression," in *IEEE Aerospace Conference*, March 2020, pp. 1–11.
- [18] ITU, "Radio regulations," 2020. [Online]. Available: <http://handle.itu.int/11.1002/pub/814b0c44-en>
- [19] M. J. Marcus, "Harmful interference and its role in spectrum policy," *Proceedings of the IEEE*, vol. 102, no. 3, pp. 265–269, March 2014.
- [20] M. M. Sohel, M. Yao, T. Yang, and J. H. Reed, "Spectrum access system for the citizen broadband radio service," *IEEE Communications Magazine*, vol. 53, no. 7, pp. 18–25, July 2015.
- [21] F. C. Commission, "Amendment of the Commission's Rules with Regard to Commercial Operations in the 3550-3650 MHz Band," FCC 15-47 A1 GN Docket No. 12-354, April 2015. [Online]. Available: <https://docs.fcc.gov/public/attachments/FCC-15-47A1.pdf>
- [22] National Research Council, *Spectrum Management for Science in the 21st Century*. National Academy Press, 2010.
- [23] ITU-R, "Performance and interference criteria for satellite passive remote sensing," Recommendation RS.2017, 2012. [Online]. Available: <https://www.itu.int/rec/R-REC-RS.2017/en>
- [24] —, "Protection criteria used for radio astronomical measurements," Recommendation RA.769-2, 2003. [Online]. Available: <https://www.itu.int/rec/R-REC-RA.769/en>
- [25] —, "Levels of data loss to radio astronomy observations and percentage-of-time criteria resulting from degradation by interference for frequency bands allocated to the radio astronomy service on a primary basis," Recommendation RA.1513-2, 2015. [Online]. Available: <https://www.itu.int/rec/R-REC-RA.1513/en>
- [26] ITU WRC-2000, "Consideration of sharing and adjacent-band compatibility between passive and active services above 71 GHz," Resolution 731 (Rev.WRC-19), 2019. [Online]. Available: https://www.itu.int/dms_pub/itu-r/oth/0C/0A/R0C0A00000F00149PDFE.pdf
- [27] I. F. Akyildiz, C. Han, Z. Hu, S. Nie, and J. M. Jornet, "Terahertz band communication: An old problem revisited and research directions

- for the next decade,” *IEEE Transactions on Communications*, vol. 70, no. 6, pp. 4250–4285, 2022.
- [28] M. Andreello, A. Singh, N. Thawdar, and J. M. Jornet, “Dynamic beamforming algorithms for ultra-directional terahertz communication systems based on graphene-based plasmonic nano-antenna arrays,” in *2018 52nd Asilomar Conference on Signals, Systems, and Computers*. IEEE, 2018, pp. 1558–1563.
- [29] US Law, “An act to provide for the regulation of interstate and foreign communication by wire or radio, and for other purposes,” Pub. L. 73-416, 1934.
- [30] M. J. Marcus, “Spectrum policy for radio spectrum access,” *Proceedings of the IEEE*, vol. 100, no. Special Centennial Issue, pp. 1685–1691, May 2012.
- [31] C. Prigent, J. R. Pardo, and W. B. Rossow, “Comparisons of the millimeter and submillimeter bands for atmospheric temperature and water vapor soundings for clear and cloudy skies,” *Journal of Applied Meteorology and climatology*, vol. 45, no. 12, pp. 1622–1633, 2006.
- [32] K. B. Cooper *et al.*, “G-band radar for humidity and cloud remote sensing,” *IEEE Transactions on Geoscience and Remote Sensing*, vol. 59, no. 2, pp. 1106–1117, 2021.
- [33] G. Skofronick-Jackson *et al.*, “The Global Precipitation Measurement (GPM) mission for science and society,” *Bulletin of the American Meteorological Society*, vol. 98, no. 8, pp. 1679–1695, 2017.
- [34] D. C. Tobin *et al.*, “Atmospheric radiation measurement site atmospheric state best estimates for atmospheric infrared sounder temperature and water vapor retrieval validation,” *Journal of Geophysical Research: Atmospheres*, vol. 111, no. D9, 2006.
- [35] B. A. McGuire, “2018 Census of Interstellar, Circumstellar, Extragalactic, Protoplanetary Disk, and Exoplanetary Molecules,” *The Astrophysical Journal Supplement Series*, vol. 239, no. 2, p. 17, Dec. 2018.
- [36] F. Combes, “Molecular gas in distant galaxies from ALMA studies,” *The Astronomy and Astrophysics Review*, vol. 26, no. 1, p. 5, Aug. 2018.
- [37] F. Norouzian, E. G. Hoare, E. Marchetti, M. Cherniakov, and M. Gashinova, “Next Generation, Low-THz Automotive Radar – the potential for frequencies above 100 GHz,” in *2019 20th International Radar Symposium (IRS)*, 2019, pp. 1–7.
- [38] J. T. Richard and H. O. Everitt, “Millimeter wave and terahertz synthetic aperture radar for locating metallic scatterers embedded in scattering media,” *IEEE Transactions on Terahertz Science and Technology*, vol. 7, no. 6, pp. 732–740, 2017.
- [39] Event Horizon Telescope Collaboration *et al.*, “First M87 Event Horizon Telescope Results. I. The Shadow of the Supermassive Black Hole,” *The Astrophysical Journal Letters*, vol. 875, no. 1, p. L1, Apr. 2019.
- [40] T. R. Hunter and R. Kimberk, “Statistical topics concerning radiometer theory,” in *Proceedings of the 26th International Symposium on Space Terahertz Technology (ISSTT)*, Cambridge, MA, 2015. [Online]. Available: <https://www.nrao.edu/meetings/isstt/papers/2015/2015000059.pdf>
- [41] A. J. Tetarenko *et al.*, “Measuring fundamental jet properties with multi-wavelength fast timing of the black hole X-ray binary MAXI J1820+070,” *Monthly Notices of the Royal Astronomical Society*, Mar. 2021.
- [42] J. Carpenter, D. Iono, F. Kemper, and A. Wootten, “The ALMA Development Program: Roadmap to 2030,” *arXiv e-prints*, p. arXiv:2001.11076, Jan. 2020.
- [43] T. S. Rappaport *et al.*, “Wireless Communications and Applications Above 100 GHz: Opportunities and Challenges for 6G and Beyond,” *IEEE Access*, vol. 7, pp. 78 729–78 757, 2019.
- [44] C. Castro, R. Elschner, T. Merkle, C. Schubert, and R. Freund, “Experimental Demonstrations of High-Capacity THz-Wireless Transmission Systems for Beyond 5G,” *IEEE Communications Magazine*, vol. 58, no. 11, pp. 41–47, November 2020.
- [45] U. R. Pfeiffer, R. Jain, J. Grzyb, S. Malz, P. Hillger, and P. Rodríguez-Vázquez, “Current status of terahertz integrated circuits - from components to systems,” in *IEEE BiCMOS and Compound Semiconductor Integrated Circuits and Technology Symposium (BCICTS)*, 2018, pp. 1–7.
- [46] N. Benvenuto, G. Cherubini, and S. Tomasin, *Algorithms for communications systems and their applications*. John Wiley & Sons, 2021.
- [47] P. Banelli, S. Buzzi, G. Colavolpe, A. Modenini, F. Rusek, and A. Ugolini, “Modulation Formats and Waveforms for 5G Networks: Who Will Be the Heir of OFDM?: An overview of alternative modulation schemes for improved spectral efficiency,” *IEEE Signal Processing Magazine*, vol. 31, no. 6, pp. 80–93, Nov 2014.
- [48] G. Berardinelli, K. Pajukoski, E. Lahetkangas, R. Wichman, O. Tirkkonen, and P. Mogensen, “On the Potential of OFDM Enhancements as 5G Waveforms,” in *2014 IEEE 79th Vehicular Technology Conference (VTC Spring)*, May 2014, pp. 1–5.
- [49] T. L. Marzetta, “Noncooperative cellular wireless with unlimited numbers of base station antennas,” *IEEE Transactions on Wireless Communications*, vol. 9, no. 11, pp. 3590–3600, November 2010.
- [50] I. F. Akyildiz and J. M. Jornet, “Realizing ultra-massive MIMO (1024 × 1024) communication in the (0.06–10) terahertz band,” *Nano Communication Networks*, vol. 8, pp. 46–54, 2016, U.S. Patent No. 9,825,712, November 21, 2017 (Priority Date: Dec. 6, 2013).
- [51] N. Rajatheva *et al.*, “Scoring the terabit/s goal: Broadband connectivity in 6G,” *arXiv preprint arXiv:2008.07220*, 2020.
- [52] S. Palicot, Y. Corre, G. Gougeon, and J.-B. Dore, “Deliverable D1.0: Beyond-5G Wireless Tbps Scenarios and Requirements,” Deliverable D1.0 - Brave Beyond 5G. [Online]. Available: <http://www.brave-beyond5g.com/wp-content/uploads/2018/12/BRAVE-D1.0-B5G-wireless-Tbps-Scenarios-and-Requirements-v1-1.pdf>
- [53] T. Kurner and T. Kawanishi, “Demonstrating 300 GHz Wireless Backhaul Links – The Thor Approach,” in *47th International Conference on Infrared, Millimeter and Terahertz Waves (IRMMW-THz)*, Aug 2022, pp. 1–1.
- [54] X. Xu, Y. Pan, P. P. M. Y. Lwin, and X. Liang, “3D holographic display and its data transmission requirement,” in *2011 International Conference on Information Photonics and Optical Communications*, Oct 2011, pp. 1–4.
- [55] S. H. Samy, E. A. Maher, A. El-Mahdy, and F. Dressler, “Power Optimization of THz Band Heterogeneous Vehicular Networks,” in *IEEE Vehicular Networking Conference (VNC)*, Nov 2021, pp. 107–114.
- [56] A. Simsek, S.-K. Kim, and M. J. Rodwell, “A 140 GHz MIMO Transceiver in 45 nm SOI CMOS,” in *IEEE BiCMOS and Compound Semiconductor Integrated Circuits and Technology Symposium (BCICTS)*, 2018, pp. 231–234.
- [57] S. Kueppers, H. Cetinkaya, and N. Pohl, “A compact 120 GHz SiGe:C based 2 × 8 FMCW MIMO radar sensor for robot navigation in low visibility environments,” in *2017 European Radar Conference (EURAD)*, Oct 2017, pp. 122–125.
- [58] ITU, “World Radiocommunication Conference (WRC-2000) outcomes and documents,” 2000. [Online]. Available: <http://handle.itu.int/11.1004/020.1000/4.126>
- [59] ITU-R, “Protection of the radio astronomy service in frequency bands shared with other services,” ITU-R Recommendation RA.1031-2, 2007. [Online]. Available: <https://www.itu.int/rec/R-REC-RA.1031-2-200706-I/en>
- [60] —, “Typical technical and operational characteristics of Earth exploration-satellite service (passive) systems using allocations between 1.4 and 275 GHz,” Recommendation RS.1861, 2010. [Online]. Available: <https://www.itu.int/rec/R-REC-RS.1861/en>
- [61] —, “Typical technical and operating characteristics and frequency bands used by space research service (passive) planetary observation systems,” ITU-R recommendation RS.2064-0, 2014. [Online]. Available: https://www.itu.int/dms_pubrec/itu-r/rec/rs/R-REC-RS.2064-0-201412-!#!PDF-E.pdf
- [62] V. Petrov, A. Pyattaev, D. Moltchanov, and Y. Koucheryavy, “Terahertz band communications: Applications, research challenges, and standardization activities,” in *8th International Congress on Ultra Modern Telecommunications and Control Systems and Workshops (ICUMT)*, Oct 2016, pp. 183–190.
- [63] ITU-R, “Calculation of free-space attenuation,” Recommendation P.525, 2019. [Online]. Available: <https://www.itu.int/rec/R-REC-P.525/en>
- [64] —, “Attenuation by atmospheric gases and related effects,” Recommendation P.676, 2019. [Online]. Available: <https://www.itu.int/rec/R-REC-P.676/en>
- [65] —, “Reference Standard Atmospheres,” Recommendation P.835, 2017. [Online]. Available: <https://www.itu.int/rec/R-REC-P.835/en>
- [66] —, “The radio refractive index: its formula and refractivity data,” Recommendation P.453, 2019. [Online]. Available: <https://www.itu.int/rec/R-REC-P.453/en>
- [67] J. F. O’Hara and D. R. Grischkowsky, “Comment on the Veracity of the ITU-R Recommendation for Atmospheric Attenuation at Terahertz Frequencies,” *IEEE Transactions on Terahertz Science and Technology*, vol. 8, no. 3, pp. 372–375, May 2018.
- [68] ITU-R, “Analytical method to calculate short-term visibility and interference statistics for non-geostationary satellite orbit satellites as seen from a point on the Earth’s surface,” Recommendation S.1257, 2002. [Online]. Available: <https://www.itu.int/rec/R-REC-S.1257/en>

- [69] —, “Reference radiation patterns for fixed wireless system antennas for use in coordination studies and interference assessment in the frequency range from 100 MHz to 86 GHz,” Recommendation F.699-8, 2018. [Online]. Available: <https://www.itu.int/rec/R-REC-F.699/en>
- [70] P. Sen, D. A. Pados, S. N. Batalama, E. Einarsson, J. P. Bird, and J. M. Jornet, “The teranova platform: An integrated testbed for ultra-broadband wireless communications at true terahertz frequencies,” *Computer Networks*, vol. 179, p. 107370, 2020. [Online]. Available: <https://www.sciencedirect.com/science/article/pii/S1389128620304473>
- [71] J. G. Proakis and M. Salehi, *Digital communications*. McGraw-Hill, 2008.
- [72] X. Ge, H. Cheng, M. Guizani, and T. Han, “5G wireless backhaul networks: challenges and research advances,” *IEEE Network*, vol. 28, no. 6, pp. 6–11, Nov 2014.
- [73] O. P. Adare, H. Babbili, C. Madapatha, B. Makki, and T. Svensson, “Uplink Power Control in Integrated Access and Backhaul Networks,” in *2021 IEEE International Symposium on Dynamic Spectrum Access Networks (DySPAN)*, Dec 2021, pp. 163–168.
- [74] M. R. Schoeberl *et al.*, “Overview of the EOS Aura mission,” *IEEE Transactions on Geoscience and Remote Sensing*, vol. 44, no. 5, pp. 1066–1074, May 2006.
- [75] C. Parkinson, “Aqua: an Earth-Observing Satellite mission to examine water and other climate variables,” *IEEE Transactions on Geoscience and Remote Sensing*, vol. 41, no. 2, pp. 173–183, Feb 2003.
- [76] P. Edwards and D. Pawlak, “MetOp: The space segment for EUMETSAT’s polar system,” *ESA bulletin*, pp. 7–18, 2000.
- [77] F. Rinaldi *et al.*, “Non-Terrestrial Networks in 5G & Beyond: A Survey,” *IEEE Access*, vol. 8, pp. 165 178–165 200, 2020.
- [78] A. J. Alqaraghuli, H. Abdellatif, and J. M. Jornet, “Performance Analysis of a Dual Terahertz/Ka Band Communication System for Satellite Mega-Constellations,” in *IEEE 22nd International Symposium on a World of Wireless, Mobile and Multimedia Networks (WoWMoM)*, June 2021, pp. 316–322.
- [79] S. Wan, J. Hu, C. Chen, A. Jolfaei, S. Mumtaz, and Q. Pei, “Fair-Hierarchical Scheduling for Diversified Services in Space, Air and Ground for 6G-Dense Internet of Things,” *IEEE Transactions on Network Science and Engineering*, pp. 1–1, 2020.
- [80] L. Bertizzolo *et al.*, “Live and Let Live: Flying UAVs Without Affecting Terrestrial UEs,” in *Proceedings of the 21st International Workshop on Mobile Computing Systems and Applications*, ser. HotMobile ’20. Austin, TX, USA: Association for Computing Machinery, 2020, p. 21–26.
- [81] European Organization for Astronomical Research in the Southern Hemisphere (ESO), “A Report on the Impact of Satellite Constellations,” arXiv:2108.03999 [astro-ph.IM]. [Online]. Available: <https://arxiv.org/pdf/2108.03999.pdf>
- [82] C. A. Balanis, *Antenna theory: analysis and design*. John Wiley & sons, 2016.
- [83] V. Jamnejad, J. Huang, B. Levitt, T. Pham, and R. Cesarone, “Array antennas for JPL/NASA deep space network,” in *Proceedings of the IEEE Aerospace Conference*, vol. 2. IEEE, 2002, pp. 2–2.
- [84] L. Zhang, M. Xiao, G. Wu, M. Alam, Y. Liang, and S. Li, “A Survey of Advanced Techniques for Spectrum Sharing in 5G Networks,” *IEEE Wireless Communications*, vol. 24, no. 5, pp. 44–51, October 2017.
- [85] F. Hu, B. Chen, and K. Zhu, “Full Spectrum Sharing in Cognitive Radio Networks Toward 5G: A Survey,” *IEEE Access*, vol. 6, pp. 15 754–15 776, 2018.
- [86] Y. Han, E. Ekici, H. Kremono, and O. Altintas, “Spectrum sharing methods for the coexistence of multiple RF systems: A survey,” *Ad Hoc Networks*, vol. 53, pp. 53–78, 2016. [Online]. Available: <https://www.sciencedirect.com/science/article/pii/S1570870516302153>
- [87] M. Fitch, M. Nekovee, S. Kawade, K. Briggs, and R. MacKenzie, “Wireless service provision in TV white space with cognitive radio technology: A telecom operator’s perspective and experience,” *IEEE Communications Magazine*, vol. 49, no. 3, pp. 64–73, March 2011.
- [88] Z. Zhang *et al.*, “6G Wireless Networks: Vision, Requirements, Architecture, and Key Technologies,” *IEEE Vehicular Technology Magazine*, vol. 14, no. 3, pp. 28–41, Sep. 2019.
- [89] L. Dai, B. Wang, Z. Ding, Z. Wang, S. Chen, and L. Hanzo, “A Survey of Non-Orthogonal Multiple Access for 5G,” *IEEE Communications Surveys Tutorials*, vol. 20, no. 3, pp. 2294–2323, Third quarter 2018.
- [90] L. Zhang, Y.-C. Liang, and M. Xiao, “Spectrum sharing for internet of things: A survey,” *IEEE Wireless Communications*, vol. 26, no. 3, pp. 132–139, June 2019.
- [91] Y. R. Ramadan, H. Minn, and Y. Dai, “A new paradigm for spectrum sharing between cellular wireless communications and radio astronomy systems,” *IEEE Transactions on Communications*, vol. 65, no. 9, pp. 3985–3999, Sep. 2017.
- [92] Y. Cho, H.-K. Kim, M. Nekovee, and H.-S. Jo, “Coexistence of 5G With Satellite Services in the Millimeter-Wave Band,” *IEEE Access*, vol. 8, pp. 163 618–163 636, 2020.
- [93] M. Marcus, X. C. Roman, and J. Jornet, “Millimeter-Wave Propagation: Spectrum Management Implications—An Update for >100 GHz [Speaker’s Corner],” *IEEE Microwave Magazine*, vol. 24, no. 1, pp. 91–94, 2023.
- [94] I. Khalifa and R. Vaughan, “Geometric design of pyramidal antenna arrays for hemispherical scan coverage,” *IEEE Transactions on Antennas and Propagation*, vol. 55, no. 2, pp. 468–471, 2007.
- [95] A. F. Molisch, V. V. Ratnam, S. Han, Z. Li, S. L. H. Nguyen, L. Li, and K. Haneda, “Hybrid beamforming for massive MIMO: A survey,” *IEEE Communications Magazine*, vol. 55, no. 9, pp. 134–141, September 2017.
- [96] S. W. Varade and K. D. Kulat, “Robust algorithms for DOA estimation and adaptive beamforming for smart antenna application,” in *2009 Second International Conference on Emerging Trends in Engineering & Technology*. IEEE, 2009, pp. 1195–1200.
- [97] M. Di Renzo *et al.*, “Smart radio environments empowered by reconfigurable AI meta-surfaces: An idea whose time has come,” *EURASIP Journal on Wireless Communications and Networking*, vol. 2019, no. 1, pp. 1–20, 2019.
- [98] N. M. Monroe, G. C. Doqjiamis, R. Stingel, P. Myers, X. Chen, and R. Han, “Electronic THz Pencil Beam Forming and 2D Steering for High Angular-Resolution Operation: A 98×98-Unit 265GHz CMOS Reflectarray with In-Unit Digital Beam Shaping and Squint Correction,” in *2022 IEEE International Solid-State Circuits Conference (ISSCC)*, vol. 65. IEEE, 2022, pp. 1–3.
- [99] M. J. Rodwell, “100-340GHz Spatially Multiplexed Communications: IC, Transceiver, and Link Design,” in *2019 IEEE 20th International Workshop on Signal Processing Advances in Wireless Communications (SPAWC)*. IEEE, 2019, pp. 1–5.
- [100] A. Singh, A. J. Alqaraghuli, and J. M. Jornet, “Wavefront engineering at terahertz frequencies through intelligent reflecting surfaces,” in *2022 IEEE 23rd International Workshop on Signal Processing Advances in Wireless Communication (SPAWC)*. IEEE, 2022, pp. 1–5.
- [101] C. Liaskos, S. Nie, A. Tsioliaridou, A. Pitsillides, S. Ioannidis, and I. Akyildiz, “A novel communication paradigm for high capacity and security via programmable indoor wireless environments in next generation wireless systems,” *Ad Hoc Networks*, vol. 87, pp. 1–16, 2019.
- [102] S. Liu *et al.*, “A review of anomalous refractive and reflective metasurfaces,” *Nanotechnology and Precision Engineering*, vol. 5, no. 2, p. 025001, 2022.
- [103] Z. Shaikhanov, S. Badran, J. M. Jornet, D. M. Mittleman, and E. W. Knightly, “Remotely positioned metasurface-drone attack,” in *Proceedings of the 24th International Workshop on Mobile Computing Systems and Applications*, 2023, pp. 110–116.
- [104] S. Sun, T. S. Rappaport, R. W. Heath, A. Nix, and S. Rangan, “MIMO for millimeter-wave wireless communications: Beamforming, spatial multiplexing, or both?” *IEEE Communications Magazine*, vol. 52, no. 12, pp. 110–121, 2014.
- [105] A. R. Vilenskiy, E. Galesloot, Y. Zhang, A. B. Smolders, and M. V. Ivashina, “Quasi-Optical Beamforming Network for Millimeter-Wave Electronically Scanned Array Antennas with 1-Bit Phase Resolution,” in *2021 15th European Conference on Antennas and Propagation (EuCAP)*. IEEE, 2021, pp. 1–5.
- [106] P.-Y. Chen and A. Alù, “THz beamforming using graphene-based devices,” in *2013 IEEE Radio and Wireless Symposium*. IEEE, 2013, pp. 55–57.
- [107] J. M. Jornet and I. F. Akyildiz, “Graphene-based plasmonic nano-transceiver for terahertz band communication,” in *Proc. of the 8th European Conference on Antennas and Propagation (EuCAP)*. IEEE, 2014, pp. 492–496, U.S. Patent No. 9,397,758, July 19, 2016 (Priority Date: Dec. 6, 2013).
- [108] J. Crabb, X. Cantos-Roman, J. M. Jornet, and G. R. Aizin, “Hydrodynamic theory of the Dyakonov-Shur instability in graphene transistors,” *Physical Review B*, vol. 104, no. 15, p. 155440, 2021.
- [109] P. K. Singh, G. Aizin, N. Thawdar, M. Medley, and J. M. Jornet, “Graphene-based plasmonic phase modulator for terahertz-band communication,” in *Proc. of the 10th European Conference on Antennas and Propagation (EuCAP)*. IEEE, 2016, pp. 1–5.
- [110] J. Crabb, X. Cantos-Roman, G. R. Aizin, and J. M. Jornet, “Amplitude and frequency modulation with an on-chip graphene-based

- plasmonic terahertz nanogenerator," *IEEE Transactions on Nanotechnology*, vol. 21, pp. 539–546, 2022.
- [111] J. M. Jornet and I. F. Akyildiz, "Graphene-based plasmonic nano-antenna for terahertz band communication in nanonetworks," *IEEE Journal on selected areas in communications*, vol. 31, no. 12, pp. 685–694, 2013, U.S. Patent No. 9,643,841, May 9, 2017 (Priority Date: Dec. 6, 2013).
- [112] A. Singh, M. Andrello, N. Thawdar, and J. M. Jornet, "Design and operation of a graphene-based plasmonic nano-antenna array for communication in the terahertz band," *IEEE Journal on Selected Areas in Communications*, vol. 38, no. 9, pp. 2104–2117, 2020.
- [113] M. H. Dahri, M. H. Jamaluddin, M. Khalily, M. I. Abbasi, R. Selvaraju, and M. R. Kamarudin, "Polarization diversity and adaptive beamsteering for 5g reflectarrays: A review," *IEEE Access*, vol. 6, pp. 19451–19464, 2018.
- [114] A. Singh, M. Andrello, E. Einarsson, N. Thawdar, and J. M. Jornet, "A hybrid intelligent reflecting surface with graphene-based control elements for THz communications," in *2020 IEEE 21st International Workshop on Signal Processing Advances in Wireless Communications (SPAWC)*. IEEE, 2020, pp. 1–5.
- [115] B. A. Munk, *Frequency selective surfaces: theory and design*. John Wiley & Sons, 2005.
- [116] M. A. Al-Joumayly and N. Behdad, "Wideband planar microwave lenses using sub-wavelength spatial phase shifters," *IEEE Transactions on Antennas and Propagation*, vol. 59, no. 12, pp. 4542–4552, 2011.
- [117] M. Li, M. A. Al-Joumayly, and N. Behdad, "Broadband true-time-delay microwave lenses based on miniaturized element frequency selective surfaces," *IEEE Transactions on Antennas and Propagation*, vol. 61, no. 3, pp. 1166–1179, 2012.
- [118] U. Nissanov, G. Singh, and N. Kumar, "High gain microstrip array antenna with SIW and FSS for beyond 5 G at THz band," *Optik*, vol. 236, p. 166568, 2021.
- [119] B. Zhang, J. M. Jornet, I. F. Akyildiz, and Z. P. Wu, "Mutual coupling reduction for ultra-dense multi-band plasmonic nano-antenna arrays using graphene-based frequency selective surface," *IEEE Access*, vol. 7, pp. 33 214–33 225, 2019.
- [120] S. Venkatesh, X. Lu, H. Saeidi, and K. Sengupta, "A high-speed programmable and scalable terahertz holographic metasurface based on tiled CMOS chips," *Nature Electronics*, pp. 1–9, 2020.
- [121] Fridman, P. A. and Baan, W. A., "RFI mitigation methods in radio astronomy," *A&A*, vol. 378, no. 1, pp. 327–344, 2001. [Online]. Available: <https://doi.org/10.1051/0004-6361:20011166>
- [122] J. E. Balling, S. S. Søjbjerg, S. S. Kristensen, and N. Skou, "RFI detected by kurtosis and polarimetry: Performance comparison based on airborne campaign data," in *12th Specialist Meeting on Microwave Radiometry and Remote Sensing of the Environment (MicroRad)*, March 2012, pp. 1–4.
- [123] D. Bradley, J. M. Morris, T. Adali, J. T. Johnson, and M. Aksoy, "On the detection of RFI using the complex signal kurtosis in microwave radiometry," in *13th Specialist Meeting on Microwave Radiometry and Remote Sensing of the Environment (MicroRad)*, March 2014, pp. 33–38.
- [124] J. R. Piepmeier *et al.*, "Radio-frequency interference mitigation for the soil moisture active passive microwave radiometer," *IEEE Transactions on Geoscience and Remote Sensing*, vol. 52, no. 1, pp. 761–775, Jan 2014.
- [125] —, "SMAP L-Band Microwave Radiometer: Instrument Design and First Year on Orbit," *IEEE Transactions on Geoscience and Remote Sensing*, vol. 55, no. 4, pp. 1954–1966, April 2017.
- [126] J. T. Johnson, P. N. Mohammed, J. R. Piepmeier, A. Bringer, and M. Aksoy, "Soil Moisture Active Passive (SMAP) microwave radiometer radio-frequency interference (RFI) mitigation: Algorithm updates and performance assessment," in *IEEE International Geoscience and Remote Sensing Symposium (IGARSS)*, July 2016, pp. 123–124.
- [127] J. Querol, A. Alonso-Arroyo, R. Onrubia, D. Pascual, and A. Camps, "Assessment of back-end RFI mitigation techniques in passive remote sensing," in *IEEE International Geoscience and Remote Sensing Symposium (IGARSS)*, July 2015, pp. 4746–4749.
- [128] L. W. Peck and D. M. Fenech, "SERPent: Automated reduction and RFI-mitigation software for e-MERLIN," *Astronomy and Computing*, vol. 2, pp. 54–66, 2013. [Online]. Available: <https://www.sciencedirect.com/science/article/pii/S2213133713000255>
- [129] Z.-S. Zhang *et al.*, "First SETI observations with china's five-hundred-meter aperture spherical radio telescope (FAST)," *The Astrophysical Journal*, vol. 891, no. 2, p. 174, mar 2020. [Online]. Available: <https://doi.org/10.3847/1538-4357/ab7376>
- [130] R. V. van Nieuwpoort, "Towards exascale real-time RFI mitigation," in *Radio Frequency Interference (RFI)*, Oct 2016, pp. 69–74.
- [131] V. Ariyaratna, A. Madanayake, and J. M. Jornet, "Real-Time Digital Baseband System for Ultra-Broadband THz Communication," in *IEEE 45th International Conference on Infrared, Millimeter, and Terahertz Waves (IRMMW-THz)*, 2020.
- [132] R. Selina, U. Rau, R. Hiriart, and A. Erickson, "RFI Mitigation in the ngVLA System Architecture ngVLA Memo# 71," 2020. [Online]. Available: https://library.nrao.edu/public/memos/ngvla/NGVLA_71.pdf
- [133] D. M. Le Vine, J. T. Johnson, and J. Piepmeier, "RFI and remote sensing of the Earth from space," in *2016 Radio Frequency Interference (RFI)*, Oct 2016, pp. 49–54.
- [134] C. Han, L. Yan, and J. Yuan, "Hybrid beamforming for terahertz wireless communications: Challenges, architectures, and open problems," *IEEE Wireless Communications*, vol. 28, no. 4, pp. 198–204, 2021.
- [135] K. S. Zigangirov, *Theory of code division multiple access communication*. John Wiley & Sons, 2004, vol. 6.
- [136] C. Bosso, P. Sen, X. Cantos-Roman, C. Parisi, N. Thawdar, and J. M. Jornet, "Ultrabroadband Spread Spectrum Techniques for Secure Dynamic Spectrum Sharing Above 100 GHz Between Active and Passive Users," in *2021 IEEE International Symposium on Dynamic Spectrum Access Networks (DySPAN)*. IEEE, 2021, pp. 45–52.
- [137] P. Sen, H. Pandey, and J. M. Jornet, "Ultra-broadband chirp spread spectrum communication in the terahertz band," in *Next-Generation Spectroscopic Technologies XIII*, vol. 11390. SPIE, 2020, pp. 7–18.
- [138] S. Aliaga, A. J. Alqaraghuli, and J. M. Jornet, "Joint terahertz communication and atmospheric sensing in low earth orbit satellite networks: Physical layer design," in *2022 IEEE 23rd International Symposium on a World of Wireless, Mobile and Multimedia Networks (WoWMoM)*. IEEE, 2022, pp. 457–463.
- [139] A. Grami, *Introduction to digital communications*. Academic Press, 2015.
- [140] P. Luethi, C. Studer, S. Duetsch, E. Zraggen, H. Kaeslin, N. Felber, and W. Fichtner, "Gram-Schmidt-based QR decomposition for MIMO detection: VLSI implementation and comparison," in *APCCAS 2008-2008 IEEE Asia Pacific Conference on Circuits and Systems*. IEEE, 2008, pp. 830–833.
- [141] C. Shi and G. Li, "Coordinated Blanking for 5G Millimeter-Wave Networks Spectrum Sharing," in *IEEE 83rd Vehicular Technology Conference (VTC Spring)*, May 2016, pp. 1–5.
- [142] M. Polese, V. Ariyaratna, P. Sen, J. V. Siles, F. Restuccia, T. Melodia, and J. M. Jornet, "Dynamic spectrum sharing between active and passive users above 100 GHz," *Communications Engineering*, vol. 1, no. 1, pp. 1–9, 2022.
- [143] B. Peng, K. Guan, A. Kuter, S. Rey, M. Patzold, and T. Kuerner, "Channel Modeling and System Concepts for Future Terahertz Communications: Getting Ready for Advances Beyond 5G," *IEEE Vehicular Technology Magazine*, vol. 15, no. 2, pp. 136–143, June 2020.
- [144] A. B. Kihero, M. S. J. Solajja, A. Yazar, and H. Arslan, "Inter-Numerology Interference Analysis for 5G and Beyond," in *IEEE Globecom Workshops (GC Wkshps)*, 2018, pp. 1–6.
- [145] N. Patriciello, S. Lagen, L. Giupponi, and B. Bojovic, "5G New Radio Numerologies and their Impact on the End-To-End Latency," in *2018 IEEE 23rd International Workshop on Computer Aided Modeling and Design of Communication Links and Networks (CAMAD)*, Sep. 2018, pp. 1–6.
- [146] M. Polese, L. Bonati, S. D'Oro, S. Basagni, and T. Melodia, "Understanding O-RAN: Architecture, Interfaces, Algorithms, Security, and Research Challenges," *IEEE Communications Surveys & Tutorials*, pp. 1–1, 2023.
- [147] R. J. Baxley and R. S. Thompson, "Deep Learning Collaborative Radios - Team Zylinium Phase 3," AFRL-RI-RS-TR-2020-158. [Online]. Available: <https://apps.dtic.mil/sti/pdfs/AD1107855.pdf>
- [148] —, "Team Zylinium DARPA Spectrum Collaboration Challenge Radio Design and Implementation," in *2019 IEEE International Symposium on Dynamic Spectrum Access Networks (DySPAN)*, Nov 2019, pp. 1–6.
- [149] PAWR Project Office (PPO), "New \$2.7M PAWR Project Funded by the U.S. Department of Defense Will Test AI-Driven Spectrum Sharing Optimization In a 5G-NR Network," PPO Press Release. [Online]. Available: <https://advancedwireless.org/new-2-7m-pawr-project-funded-by-the-us-department-of-defense-will-test-ai-driven-spectrum-sharing-optimization-in-a-5g-nr-network/>
- [150] E. Eichen, "Real-Time Geographical Spectrum Sharing by 5G Networks and Earth Exploration Satellite Services," in *IEEE International Symposium on Dynamic Spectrum Access Networks (DySPAN)*, Nov 2019, pp. 1–2.

- [151] L. Bonati *et al.*, "Colosseum: Large-scale wireless experimentation through hardware-in-the-loop network emulation," in *IEEE International Symposium on Dynamic Spectrum Access Networks (DySPAN)*, Dec 2021, pp. 105–113.



Michele Polese (S'17, M'20) is a Principal Research Scientist at Northeastern University, Boston, since March 2020. He received his Ph.D. at the Department of Information Engineering of the University of Padova in 2020 under the supervision of with Michele Zorzi. He also was an adjunct professor and postdoctoral researcher in 2019/2020 at the University of Padova, and a part-time lecturer in Fall 2020 and 2021 at Northeastern University. During his Ph.D., he visited New York University (NYU), AT&T Labs in Bedminster, NJ, and Northeastern

University. He collaborated with several academic and industrial research partners, including Intel, InterDigital, NYU, AT&T Labs, University of Aalborg, King's College and NIST. He was awarded with several best paper awards, and is serving as TPC co-chair for WNS3 2021-2022 and as an Associate Technical Editor for the *IEEE Communications Magazine*. His research interests are in the analysis and development of protocols and architectures for future generations of cellular networks (5G and beyond), in particular for millimeter-wave communication, and in the performance evaluation of complex networks.



Xavier Cantos-Roman (Student Member, IEEE) received the B.S. in Telecommunications Technologies and Services Engineering from the Universitat Politècnica de Catalunya, Barcelona, Spain, in 2019. He is a member of the Ultra-broadband Nanonetworking Laboratory at Northeastern University, Boston, MA, where he is currently a Ph.D. candidate under the guidance of Dr. Josep M. Jornet. His research interests include the modeling and simulation of THz plasmonic devices, the study of mmWave and THz signals propagation and the

design and experimental demonstration of joint communication and sensing systems at sub-THz frequencies.



Arjun Singh (Member, IEEE) received the B.S. summa cum laude, and M.S. in Electrical Engineering from the University at Buffalo, The State University of New York, NY, USA, in 2016 and 2018, respectively. He obtained his Ph.D. in Electrical Engineering from Northeastern University, Boston, USA, under the guidance of Dr. Josep Jornet, as a member of the Ultra-Broadband Nanonetworking Laboratory, in December, 2021. Since 2022, he is an Assistant Professor in the Department of Engineering at the State University of New York Polytechnic

Institute, Utica, NY. His research interests include realizing Terahertz-band wireless communications, dynamic spectrum sharing, space networks, wavefront engineering, graphene-plasmonics, and intelligent reflecting surfaces. In these areas, he has coauthored several publications in leading journals, as well as 1 US patent. He is also serving as the media chair for the IEEE RCC Special Interest Group on Terahertz Communications and as a reviewer for reputed journals including *IEEE communications magazine*.



Michael Marcus (F'04) is Director of Marcus Spectrum Solutions, Cabin John, Maryland and adjunct professor at Northeastern University's Department of Electrical and Computer Engineering, Boston, MA. He retired from the Federal Communications Commission in 2004 after nearly 25 years in senior spectrum policy positions. While at FCC, he proposed and directed the policy developments that resulted in the bands used by Wi-Fi, Bluetooth, and licensed and unlicensed millimeter wave systems above 59 GHz. He was an exchange visitor from FCC to the

Japanese spectrum regulator (now MIC) and has been a consultant to the European Commission and the Singapore regulator (now IMDA). During 2012-13 he was chair of the IEEE-USA Committee on Communication Policy and is now its vice chair for spectrum policy. In 2013, he was awarded the IEEE ComSoc Award for Public Service in the Field of Telecommunications "for pioneering spectrum policy initiatives that created modern unlicensed spectrum bands for applications that have changed our world". He received S.B. and Sc.D. degrees in electrical engineering from MIT.



Thomas J. Maccarone was born on August 26, 1974, in Haverhill, Massachusetts in the USA. He received a BS in physics from the California Institute of Technology in 1996, MS and MPhil degrees in 199 and a PhD in 2001 from Yale University in astronomy. After postdoctoral fellowships at the Scuola Internazionale Superiore di Studi Avanzati in Trieste, Italy and the University of Amsterdam, he was a lecturer then reader in the School of Physics of Astronomy at the University of Southampton from 2005-2012. In 2013, he moved to Texas Tech

University as an associate professor in the Department of Physics to help start the university's astrophysics research program, and now is Presidential Excellence in Research Professor in its Department of Physics & Astronomy. His main area of research is understanding the physics of accretion and radio jet production in X-rays binaries as well as the processes of binary formation and evolution for these systems. He has been heavily involved in efforts to plan the science cases for a wide range of new observational facilities. He serves on advisory panels to the National Radio Astronomy Observatory and the Executive Committee of the High Energy Astrophysics Division of the American Astronomical Society.



Tommaso Melodia (F'18) is the William Lincoln Smith Chair Professor with the Department of Electrical and Computer Engineering at Northeastern University, Boston. He is also the Founding Director of the Institute for the Wireless Internet of Things. He received his Ph.D. in Electrical and Computer Engineering from the Georgia Institute of Technology in 2007. He is a recipient of the NSF CAREER award. Prof. Melodia has served as Associate Editor of *IEEE Transactions on Wireless Communications*, *IEEE Transactions on Mobile Computing*, *Elsevier*

Computer Networks, among others. He has served as Technical Program Committee Chair for IEEE Infocom 2018, General Chair for IEEE SECON 2019, ACM Nanocom 2019, and ACM WUWnet 2014. Prof. Melodia is the Director of Research for the Platforms for Advanced Wireless Research (PAWR) Project Office, a \$100M public-private partnership to establish 4 city-scale platforms for wireless research to advance the US wireless ecosystem in years to come. Prof. Melodia's research on Internet-of-Things and wireless networked systems has been funded by the National Science Foundation, the Air Force Research Laboratory the Office of Naval Research, DARPA, and the Army Research Laboratory. Prof. Melodia is a Fellow of the IEEE and a Senior Member of the ACM.



Josep Miquel Jornet (M'13, SM'20) is an Associate Professor in the Department of Electrical and Computer Engineering, the director of the Ultra-broadband Nanonetworking (UN) Laboratory, and a member of the Institute for the Wireless Internet of Things and the SMART Center at Northeastern University (NU). He received a Degree in Telecommunication Engineering and a Master of Science in Information and Communication Technologies from the Universitat Politècnica de Catalunya, Spain, in 2008. He received the Ph.D. degree in Electrical and

Computer Engineering from the Georgia Institute of Technology, Atlanta, GA, in August 2013. His core research is in terahertz communications, in addition to wireless nano-bio-communication networks and the Internet of Nano-Things. In these areas, he has co-authored more than 220 peer-reviewed scientific publications, including 1 book and 5 US patents. His work has received more than 13,800 citations (h-index of 54 as of December 2022). He is serving as the lead PI on multiple grants from U.S. federal agencies including the National Science Foundation, the Air Force Office of Scientific Research and the Air Force Research Laboratory as well as industry. He is the recipient of multiple awards from IEEE and ACM as well as four best paper awards. He is a senior member of the IEEE and an IEEE ComSoc Distinguished Lecturer (Class of 2022-2023). He is also the Editor in Chief of the Elsevier Nano Communication Networks journal and Editor for IEEE Transactions on Communications.